J. Fluid Mech. (2001), *vol.* 430, *pp.* 51–86. Printed in the United Kingdom

Attenuation of sound in concentrated suspensions: theory and experiments

By PETER D. M. SPELT[1]†, MICHAEL A. NORATO[1], ASHOK S. SANGANI[1]‡, MARGARET S. GREENWOOD[2] AND LAWRENCE L. TAVLARIDES[1]

[1]Department of Chemical Engineering and Materials Science, Syracuse University, Syracuse, NY 13244, USA

[2]Pacific Northwest National Laboratory, Battelle Memorial Institute, Richland, WA 99352, USA

(Received 26 February 1999 and in revised form 6 September 2000)

Ensemble-averaged equations are derived for small-amplitude acoustic wave propagation through non-dilute suspensions. The equations are closed by introducing effective properties of the suspension such as the compressibility, density, viscoelasticity, heat capacity, and conductivity. These effective properties are estimated as a function of frequency, particle volume fraction, and physical properties of the individual phases using a self-consistent, effective-medium approximation. The theory is shown to be in excellent agreement with various rigorous analytical results accounting for multiparticle interactions. The theory is also shown to agree well with the experimental data on concentrated suspensions of small polystyrene particles in water obtained by Allegra & Hawley and for glass particles in water obtained in the present study.

1. Introduction

We consider the problem of predicting the attenuation of sound waves propagating through suspensions. When the particle volume fraction in the suspension is very small the particle interactions may be neglected and the attenuation can be determined as a function of the sound wave frequency by examining the interaction of a single particle with the incident wave as has been done by a number of investigators in the past. For example, Carstensen & Foldy (1947) examined the problem of dilute bubbly liquids while Epstein & Carhart (1953) and Allegra & Hawley (1972) examined, respectively, the case of dilute emulsions and dilute slurries. Since the attenuation behaviour is strongly dependent on the particle radius, the attenuation–frequency data for dilute suspensions may be used for determining the particle size distribution as shown by Duraiswami, Prabhukumar & Chahine (1998), who considered the case of bubbly liquids. The corresponding problem for dilute suspensions has been examined by Spelt *et al.* (1999).

The particle interactions can have a significant effect on the acoustic behaviour of non-dilute suspensions and at present rigorous calculations accounting for these interactions are lacking. Direct attack on the problem, i.e. solving the linearized

† Present address: Centre for Composite Materials, Imperial College, Prince Consort Road, London SW7 2BY, UK.

‡ Author to whom correspondence should be addressed: e-mail asangani@syr.edu

energy, momentum, and continuity equations for multiparticle systems, appears to be a daunting task even with the development of efficient computers. Thus, it is necessary to develop a suitable approximate theory and to assess its validity by comparison with the experimental data obtained with different kinds of suspensions.

We use the method of ensemble averaging to derive linearized continuity, momentum, and energy equations for the suspensions. These equations are closed by introducing effective properties of the suspensions, namely the effective conductivity, viscosity (or viscoelasticity), compressibility, and density. To estimate these properties as a function of frequency and physical properties and volume fractions of the individual phases, we must determine the relation between the conditionally averaged temperature and velocity fields inside a test particle and the temperature and velocity fields of the suspension. A self-consistent, effective-medium approximation is used for this purpose.

The predictions of the theory are compared with several known rigorous analytical calculations accounting for multiparticle interactions in dense suspensions in the limiting case of relatively small frequencies for which the acoustic wavelength is large compared with the particle radius. At very low frequencies, for which the thermal and viscous (Stokes) lengths become large compared with the particle radius, we expect the velocity and temperature fields to satisfy, respectively, the Stokes and Laplace equations. The effective properties such as the viscosity, conductivity, and permeability, for monodisperse suspensions in this limit are well-established (e.g. Ladd 1990; Mo & Sangani 1994). It is shown that the effective-medium approximation is in excellent agreement with these results. For moderate frequencies, at which the Stokes layer is very small compared with the particle radius and the wavelength is large compared with the radius, the velocity field satisfies the Laplace equation outside the Stokes layers. Added mass and Basset force coefficients, which contribute to the effective density of the suspension, have been determined by Sangani, Zhang & Prosperetti (1991) for this limiting case. Once again, the effective-medium predictions are shown to be in excellent agreement with these rigorous calculations.

We also compare the predictions of the theory with the experimental data on attenuation. Probably the best data in the literature are due to Allegra & Hawley (1972) who measured attenuation in a polystyrene–water system at frequencies for which the thermal effects contribute most significantly to the attenuation. Our theory is shown to be in excellent agreement with their data. To test the theory for the cases in which the attenuation due to viscous and scattering effects is significant, we have measured attenuation in glass–water and glass–water/glycerol systems at small to intermediate frequencies. For smaller particles, for which the viscous attenuation dominates, the theory and experiments are in very good agreement with each other. For larger particles, for which the scattering dominates, the agreement is very good only up to about 30% volume fractions.

The organization of the rest of the paper is as follows. In § 2 we derive rigorous average equations for linear acoustics and introduce effective properties of the suspensions. In § 3 we compare the predictions of the effective-medium theory with various analytical results and show how the effective properties vary with the frequency and particle volume fraction. Section 4 describes the experimental set-up used for obtaining attenuation data. Section 5 gives a comparison between the theory and various experimental data. In § 6 we present some results on the phase speed of sound waves, and discuss the possibility of using phase speed measurements for measuring particle volume fractions. Finally, § 7 summarizes important findings of the study.

2. Theory

2.1. *Linearized equations*

Let us consider a small-amplitude plane acoustic wave with frequency ω propagating through a uniform, monodisperse suspension of solid particles of radius a. We write the density as $\rho + \rho' e^{-i\omega t}$, the temperature as $T + T' e^{-i\omega t}$, and the velocity as $\boldsymbol{u} e^{-i\omega t}$. A note regarding the notation: both the equilibrium and small fluctuation values are important for the density and temperature and we therefore use primes to denote the amplitudes of the fluctuations in these quantities. Only the amplitudes of the velocity and the other field variables (stress, heat flux, etc.) will be needed, and we denote the amplitudes of these quantities without a prime so that the resulting equations look less cluttered. When the amplitudes ρ', T' and $\boldsymbol{u}$ are small, the terms involving the products of these quantities can be neglected from the continuity, momentum, and energy equations to obtain the following linearized equations:

$$-i\omega\rho' + \rho\nabla\cdot\boldsymbol{u} = 0, \tag{1}$$

$$-i\omega\rho u_i = \frac{\partial\sigma_{ij}}{\partial x_j}, \tag{2}$$

$$-i\omega\rho C_v T' = -\frac{\partial q_j}{\partial x_j} - \rho C_v \beta^{-1}(\gamma - 1)\nabla\cdot\boldsymbol{u}. \tag{3}$$

In writing the last equation, we have made use of the linearized equation of state to eliminate the pressure from the usual energy equation. The stress tensor amplitude σ_{ij} for a Newtonian fluid is given by

$$\sigma_{ij} = \left[\left\{-\frac{c^2\rho}{i\omega\gamma} + \mu_v\right\}\nabla\cdot\boldsymbol{u} - \left\{\frac{\rho(\gamma-1)C_v}{\beta T}\right\}T'\right]\delta_{ij} + d_{ij} \tag{4}$$

where d_{ij} is the deviatoric stress amplitude

$$d_{ij} = \mu\left[\frac{\partial u_i}{\partial x_j} + \frac{\partial u_j}{\partial x_i} - \tfrac{2}{3}\delta_{ij}\nabla\cdot\boldsymbol{u}\right]. \tag{5}$$

C_v is the constant volume specific heat, $\gamma = C_p/C_v$ is the ratio of specific heats, μ and μ_v are, respectively, the shear and bulk coefficients of viscosity, c is the adiabatic sound speed through the fluid, and β is the coefficient of thermal expansion. Note that the first and the third terms inside the square brackets on the right-hand side of (4) are related to the thermodynamic pressure amplitude:

$$p' = \left(\frac{\partial p}{\partial\rho}\right)_T \rho' + \left(\frac{\partial p}{\partial T}\right)_\rho T' = \frac{c^2}{\gamma}\rho' + \frac{\rho(\gamma-1)C_v}{\beta T}T'. \tag{6}$$

Finally, $q_j = -\kappa\partial T'/\partial x_j$ in (3) is the heat flux amplitude, κ being the thermal conductivity.

Inside the solid particles equations similar to (1)–(3) apply with the stress tensor given by (Landau & Lifschitz 1986)

$$\sigma_{ij} = \left[\left\{\frac{\tilde{\lambda} + \frac{2}{3}\tilde{\mu}}{-i\omega}\right\}\nabla\cdot\boldsymbol{u} - \left\{\frac{\rho(\gamma-1)C_v}{\beta T}\right\}T'\right]\delta_{ij} + \tilde{d}_{ij}, \tag{7}$$

where $\tilde{\lambda}$ and $\tilde{\mu}$ are the Lamé constants for the particles which are assumed to be perfectly elastic. Note that for solids it is customary to write the stress in terms of displacement instead of velocity. For small-amplitude oscillatory motions the

amplitudes of the two are, of course, related by a factor of $1/(-\mathrm{i}\omega)$, and this fact has been used in writing the first term on the right-hand side of the above equation. Note also that the factor $\tilde{\lambda}+(2/3)\tilde{\mu}$ is the bulk modulus of the solid. Thus, the isotropic part of the stress tensor represented by the terms inside the square brackets in the above equation arises from the density and temperature changes in the solid. The deviatoric stress tensor $\tilde{d}_{ij}$ is defined in the manner similar to (5), with the fluid viscosity replaced by the 'particle viscosity', $\mu_p = \tilde{\mu}/(-\mathrm{i}\omega)$. Note that the Lamé constant $\tilde{\mu}$ is sometimes referred to as the shear modulus.

The above linearized equations must be solved subject to the boundary conditions of continuity of velocity, temperature, heat flux, and traction ($\sigma_{ij}n_j$, n_j being the unit outward normal at the particle surface) at the interface between the particles and the fluid. In concentrated suspensions particle interactions are significant and the rigorous evaluation of sound speed and attenuation through the suspension would require the very difficult task of solving the above set of equations in a domain containing many particles.

The problem as outlined here involves a number of variables. It may be possible to simplify it in some limiting cases of small or large frequencies or when the physical properties (e.g. density and compressibility) of the two phases are widely different as in the case of acoustic propagation in bubbly liquids (Prosperetti 1984). However, it is desirable to measure the attenuation over a wide range of frequencies in order to characterize the suspension, and for most solid–liquid suspensions the ratio of physical properties does not differ significantly from unity. Thus, it is necessary to solve the full problem as described above.

2.2. *Ensemble-averaged linearized equations for suspensions*

In this subsection we ensemble-average the equations for the amplitudes of density, velocity, and temperature in the fluid and solid phases, and obtain thereby the linearized continuity, momentum, and energy equations for the suspension. It will be shown that the resulting equations have a form similar to the equations for a single phase provided that the suspension is assigned suitable properties, which we refer to as the effective properties of the suspensions. An important outcome of the averaging process will be that it will yield rigorous expressions for various effective properties of the suspension. Unlike the case of single-phase fluids, the effective properties will be seen to be functions of the wave frequency, and the equations we derive are therefore restricted to small-amplitude sinusoidal acoustic waves.

Let us denote by $g(\boldsymbol{x})$ the particle indicator function defined to be unity when the point $\boldsymbol{x}$ is inside any of the particles and zero when $\boldsymbol{x}$ is in the fluid. The properties and field variables of the liquid and particles will be denoted by subscripts l and p, respectively. The ensemble-averaged variables will be denoted by angular brackets.

Multiplying the continuity equation for the liquid by the liquid indicator function $1-g$ and for the particle by g, adding the two, and averaging the resulting equation we obtain the continuity equation for the suspension:

$$-\mathrm{i}\omega\langle\rho'\rangle + \rho_l\langle(1-g)\nabla\cdot\boldsymbol{u}_l\rangle + \rho_p\langle g\nabla\cdot\boldsymbol{u}_p\rangle = 0. \tag{8}$$

The last two terms on the left-hand side of the above equation must now be expressed in terms of the divergence of the average velocity, i.e. $\nabla\cdot\langle\boldsymbol{u}\rangle$, so that the resulting equation resembles the continuity equation of a single-phase medium (cf. (1)). We begin with the identity

$$\rho_l\langle(1-g)\nabla\cdot\boldsymbol{u}_l\rangle + \rho_p\langle g\nabla\cdot\boldsymbol{u}_p\rangle = \rho_l\nabla\cdot\langle\boldsymbol{u}\rangle + (\rho_p-\rho_l)\langle g\nabla\cdot\boldsymbol{u}_p\rangle + \rho_l\langle(\boldsymbol{u}_l-\boldsymbol{u}_p)\cdot\nabla g\rangle. \tag{9}$$

The gradient of the indicator function is zero at all points except at the particle–fluid interface where it is proportional to the Dirac delta function owing to the step jump in g across the particle–fluid interface. More specifically,

$$\nabla g = -\boldsymbol{n}\delta(\boldsymbol{x} - \boldsymbol{x}_s), \tag{10}$$

where $\boldsymbol{x} = \boldsymbol{x}_s$ represents the surface of the particles, δ is the Dirac delta function, and $\boldsymbol{n}$ is the unit normal vector, pointing into the fluid, at the particle surface.

Because the velocity is continuous across the solid–fluid interfaces, the last term in (9) vanishes; the second term on the right-hand side contains an as yet unknown quantity, $\langle g\nabla \cdot \boldsymbol{u}_p \rangle$, which is related to the average amplitude of the dilatation rate inside the particles. We shall restrict our analysis to the suspensions which are isotropic on a macroscale. For such suspensions the above quantity will be expected to be proportional to the amplitude of other scalar quantities such as $\nabla \cdot \langle \boldsymbol{u} \rangle$, the average amplitude for the mixture dilatation rate. We therefore introduce the closure relation

$$\langle g(\boldsymbol{x})(\nabla \cdot \boldsymbol{u}_p)(\boldsymbol{x}) \rangle = \phi \lambda_\rho \nabla \cdot \langle \boldsymbol{u} \rangle(\boldsymbol{x}), \tag{11}$$

where ϕ is the volume fraction of the solids. The passage of a wave will induce non-zero amplitudes of other scalar quantities such as $\langle T' \rangle$ and $\langle \sigma_{kk} \rangle$ also, and one may write a more general expression in which the average particle dilatation rate is expressed as a linear combination of all these scalar variables. In that case one must determine separately how variation in temperature, pressure and density affect separately the dilatation inside the particles. However, since all these scalar variables will be related to each other through algebraic relations that depend on the frequency and effective wavenumbers for the special case of sinusoidal acoustic waves, it is unnecessary to decompose the particle dilatation into various terms. Likewise, the dilatation rate for particles may also depend on the higher-order scalar derivatives such as $\nabla^2 \nabla \cdot \langle \boldsymbol{u} \rangle$. Since the average equations for the suspension are expected to obey wave equations, the Laplacian of the average dilatation rate can always be written in terms of the dilatation rate and the effective wavenumbers. Thus, it will suffice to use (11) for the dilatation rate inside the particles keeping in mind that λ_ρ must be evaluated such that it accounts for not only the first derivative of the suspension velocity, but also its higher-order derivatives and temperature and pressure. The calculation for λ_ρ to be presented in the next section does account for all these effects.

We note that in the present study we are interested in deriving a dispersion relation for the passage of small-amplitude acoustic waves through a suspension, and not a set of average equations valid for all suspension flows. The latter can indeed be a daunting task as equations such as (11) will not apply to the general case for which, as mentioned above, the effects of temperature, pressure, etc. must all be written separately, and the closure relation will possibly also include the higher-order derivatives. The procedure, however, is general enough in the sense that it can be used to determine the dispersion relation for other small-amplitude acoustic problems. For example, it can also be used for determining the dispersion relation for fluid-saturated porous media, which are sometimes modelled as fixed beds. Note that for the fixed bed case although the average particle velocity $\langle \boldsymbol{u}_p \rangle \equiv \langle g\boldsymbol{u}_p \rangle / \phi$ is zero, the left-hand side of (11), and hence λ_ρ, are non-zero. The radial oscillations of the fixed particles will contribute to λ_ρ in such a situation. Note that $\nabla \cdot \langle \boldsymbol{u} \rangle$ is non-zero in all acoustic problems.

Substituting for $\langle g\nabla \cdot \boldsymbol{u}_p \rangle$ from (11) into (9) yields the continuity equation for the

suspension given by

$$-\mathrm{i}\omega\langle\rho'\rangle + \rho_{c,e}\nabla\cdot\langle\boldsymbol{u}\rangle = 0, \tag{12}$$

with the effective equilibrium density of the suspension to be used in the suspension continuity equation, i.e. $\rho_{c,e}$, given by

$$\rho_{c,e} = \rho_l + (\rho_p - \rho_l)\phi\lambda_\rho. \tag{13}$$

Physically, λ_ρ represents the ratio of average dilatation amplitude in the particle phase to that in the fluid–particle mixture or the suspension. This coefficient will depend, in addition to wave frequency, on the compressibilities of both phases, volume fraction, spatial distribution of the particles, and other variables appearing in the governing equations listed in the previous subsection. Thus, we see that, in general, the effective equilibrium density of the suspension to be used in the suspension continuity equation cannot be given by some arbitrary mixture rule, e.g. the volume-averaged density or the mass-averaged density. An approximate scheme for estimating λ_ρ will be described in § 2.4.

We now proceed to derive the momentum equation for the suspension starting from (2) and its counterpart for the particles. Using the same procedure as in the continuity equation we obtain

$$-\mathrm{i}\omega\rho_{m,e}\langle u_i\rangle = \left\langle g\frac{\partial\sigma_{ij,p}}{\partial x_j}\right\rangle + \left\langle (1-g)\frac{\partial\sigma_{ij,l}}{\partial x_j}\right\rangle. \tag{14}$$

The effective (equilibrium) density of the suspension to be used in the momentum equation, $\rho_{m,e}$, is given by

$$\rho_{m,e} = \rho_l + (\rho_p - \rho_l)\phi\lambda_v \tag{15}$$

with the coefficient λ_v defined by

$$\phi\lambda_v\langle\boldsymbol{u}\rangle(\boldsymbol{x}) = \langle g(\boldsymbol{x})\boldsymbol{u}_p(\boldsymbol{x})\rangle. \tag{16}$$

Physically, λ_v represents the ratio of average velocity amplitude inside the particles to that in the suspension. Once again this coefficient, and other such coefficients to be introduced in this subsection, will, in general, depend on complex multiparticle interactions, and the details of its evaluation will be described later.

The right-hand side of (14) can be simplified using the identity

$$\begin{aligned}\frac{\partial\langle\sigma_{ij}\rangle}{\partial x_j} &\equiv \frac{\partial}{\partial x_j}\langle g\sigma_{ij,p} + (1-g)\sigma_{ij,l}\rangle \\ &= \left\langle g\frac{\partial\sigma_{ij,p}}{\partial x_j}\right\rangle + \left\langle (1-g)\frac{\partial\sigma_{ij,l}}{\partial x_j}\right\rangle + \left\langle (\sigma_{ij,p}-\sigma_{ij,l})\frac{\partial g}{\partial x_j}\right\rangle.\end{aligned} \tag{17}$$

The last term in the above equation, being related to the jump in the traction across the interface, vanishes owing to the boundary condition $\sigma_{ij,p}n_j = \sigma_{ij,l}n_j$ at the particle–fluid interface. Thus, we see that the right-hand side of (14) simply equals the divergence of the average stress in the suspension, i.e. the momentum equation for the suspension is given by

$$-\mathrm{i}\omega\rho_{m,e}\langle u_i\rangle = \frac{\partial\langle\sigma_{ij}\rangle}{\partial x_j}. \tag{18}$$

We must supplement the above momentum equation with an expression for the average stress. The linearity of the equations implies that the stress amplitude will be linear in the gradient of average velocity amplitude and $\langle T'\rangle$.

Let us first consider the isotropic part of the average stress or, equivalently, the stress trace. Multiplying the isotropic part in (4) by $1-g$ and that in (7) by g and averaging, we obtain

$$\tfrac{1}{3}\langle\sigma_{kk}\rangle = \left\{\frac{\langle c^2\rho\gamma^{-1}\rangle_e}{-\mathrm{i}\omega} + \mu_{v,e}\right\}\nabla\cdot\langle\boldsymbol{u}\rangle - T^{-1}\left\langle\rho(\gamma-1)C_v\beta^{-1}\right\rangle_{m,e}\langle T'\rangle \tag{19}$$

with

$$\langle c^2\rho\gamma^{-1}\rangle_e = c_l^2\rho_l/\gamma_l + \phi\lambda_\rho\left[\left\{\tilde{\lambda}+2\tilde{\mu}/3\right\} - c_l^2\rho_l/\gamma_l\right], \tag{20}$$

$$\mu_{v,e} = \mu_v(1-\phi\lambda_\rho), \tag{21}$$

and

$$\left\langle\rho(\gamma-1)C_v\beta^{-1}\right\rangle_{m,e} = \rho_l(\gamma_l-1)C_{v,l}\beta_l^{-1} + \phi\lambda_T\left(\rho_p(\gamma_p-1)C_{v,p}\beta_p^{-1} - \rho_l(\gamma_l-1)C_{v,l}\beta_l^{-1}\right). \tag{22}$$

The coefficient λ_ρ was defined earlier (cf. (11)). λ_T, on the other hand, is a new coefficient which is defined as the ratio of average temperature amplitude inside the particles to that in the mixture, i.e.

$$\phi\lambda_T\langle T'\rangle(\boldsymbol{x}) = \langle g(\boldsymbol{x})T_p'(\boldsymbol{x})\rangle. \tag{23}$$

Both the effective $c^2\rho/\gamma$ and the bulk viscosity of the suspension depend on the coefficient λ_ρ. This is not surprising since both depend on the average dilatation amplitude inside the particles. The result that the effective bulk viscosity $\mu_{v,e}$ of the suspension depends only on the bulk viscosity of the fluid may appear strange at first sight, but it is really a consequence of the way the isotropic part of the stress is defined for the liquid and solids (cf. (4) and (7)). The stress arising from the thermal expansion or, equivalently, temperature fluctuations depends on $\rho(\gamma-1)C_v/\beta T$ of the two phases and the relative temperature fluctuations in the two phases.

Since the deviatoric stress amplitudes in the individual phases depend only on the velocity gradient amplitude, we expect the average deviatoric stress to be linear in the gradient of average velocity amplitude. It also must be traceless. If we further assume that the suspension is macroscopically isotropic, then the average deviatoric stress is characterized by a single effective (shear) viscosity, μ_e. Thus, we write

$$\langle d_{ij}\rangle = \mu_e\left(\frac{\partial\langle u_i\rangle}{\partial x_j} + \frac{\partial\langle u_j\rangle}{\partial x_i} - \tfrac{2}{3}\delta_{ij}\nabla\cdot\langle\boldsymbol{u}\rangle\right). \tag{24}$$

To obtain an expression for the effective viscosity we need to evaluate only one component of the average deviatoric stress. We shall take, without loss of generality, the mean velocity amplitude to be given by

$$\langle\boldsymbol{u}\rangle(\boldsymbol{x}) = -\nabla\mathrm{e}^{\mathrm{i}\boldsymbol{k}_{ce}\cdot\boldsymbol{x}} = -\mathrm{i}\boldsymbol{k}_{ce}\mathrm{e}^{\mathrm{i}\boldsymbol{k}_{ce}\cdot\boldsymbol{x}}, \tag{25}$$

where $\boldsymbol{k}_{ce}$ is the effective wavenumber vector for the compressional wave through the suspension. We shall choose this vector to be aligned along the x_1-axis. The 11-component of the deviatoric stress is given by

$$\langle d_{11}\rangle = 2\left\langle\mu\frac{\partial u_1}{\partial x_1}\right\rangle - \frac{2}{3}\left\langle\mu\frac{\partial u_k}{\partial x_k}\right\rangle. \tag{26}$$

The last term on the right-hand side of the above equation, being related to the dilatation amplitudes, can be readily related to the coefficient λ_ρ introduced earlier.

The first term on the right-hand side can be expressed in terms of a coefficient λ_d defined by

$$\phi\lambda_d \frac{\partial\langle u_1\rangle}{\partial x_1} = \left\langle g(\boldsymbol{x})\frac{\partial u_1^p}{\partial x_1}(\boldsymbol{x})\right\rangle. \tag{27}$$

With this definition it is straightforward now to relate $\langle d_{11}\rangle$ to the gradient in velocity amplitude:

$$\langle d_{11}\rangle = 2\left[\mu_l + \phi\lambda_d\left(\mu_p - \mu_l\right)\right]\frac{\partial\langle u_1\rangle}{\partial x_1} - \tfrac{2}{3}\left[\mu_l + \phi\lambda_\rho\left(\mu_p - \mu_l\right)\right]\frac{\partial\langle u_k\rangle}{\partial x_k}. \tag{28}$$

Substituting for $\langle\boldsymbol{u}\rangle$ from (25) in (28) and in (24) with $i = j = 1$ and comparing the resulting expressions yields the following expression for the effective viscosity:

$$\mu_e = \mu_l + \tfrac{1}{2}\phi(\mu_p - \mu_l)\left(3\lambda_d - \lambda_\rho\right). \tag{29}$$

Finally, the energy equation for the suspension, obtained by averaging $1-g$ times the energy equation for the liquid plus g times that for the solid, is given by

$$-\mathrm{i}\omega\langle\rho C_v\rangle_e\langle T'\rangle = -\frac{\partial\langle q_j\rangle}{\partial x_j} - \left\langle\rho C_v\beta^{-1}(\gamma-1)\right\rangle_{e,e}\nabla\cdot\langle\boldsymbol{u}\rangle. \tag{30}$$

Here an argument similar to (17) has been used to simplify the energy-flux term (thereby using the boundary condition at the particle surface that the heat flux is continuous). In (30) the effective heat capacity of the suspension is given by

$$\langle\rho C_v\rangle_e = \rho_l C_{v,l} + \phi\lambda_T\left(\rho_p C_{v,p} - \rho_l C_{v,l}\right) \tag{31}$$

with λ_T defined by (23). The effective property $\langle\rho C_v(\gamma-1)\beta^{-1}\rangle_{e,e}$ appearing in the last term on the right-hand side of (30) is related to λ_ρ, and the expression for evaluating it is obtained by replacing λ_T in (22) by λ_ρ.

The average heat flux amplitude is written as

$$\langle q_j\rangle = -\kappa_e\frac{\partial\langle T'\rangle}{\partial x_j} \tag{32}$$

with the effective conductivity

$$\kappa_e = \kappa_l + \phi\lambda_\kappa\left(\kappa_p - \kappa_l\right), \tag{33}$$

where the coefficient λ_κ is the ratio of the average temperature gradient amplitude inside the particles to that in the suspension, i.e.

$$\phi\lambda_\kappa\frac{\partial\langle T'\rangle}{\partial x_i} = \left\langle g(\boldsymbol{x})\frac{\partial T_p'}{\partial x_i}(\boldsymbol{x})\right\rangle. \tag{34}$$

In summary, the continuity, momentum, and energy equations for the suspension are given by (8), (18) and (30), the average stress tensor by (19) and (24), and the average heat flux by (32). These equations resemble the equations for the single phase given in § 2.1 with suitably defined effective properties of the suspension. It must be noted that these equations are rigorous for small-amplitude sinusoidal waves through any suspension. The effective properties of the suspension will be functions of frequency and physical properties of the two phases as well as the microstructure of the suspension. Note also that properties such as $\rho_{c,e}$, the effective density to be used in the suspension continuity equation, will not depend only on the density and compressibility of the two phases but also on their thermal properties since its determination will require solving all the microscale equations simultaneously.

2.3. *Wave equations for the suspension*

To find an expression for the attenuation of sound waves in a suspension it is necessary to derive wave equations from the linearized acoustic equations for the suspension as was done by Epstein & Carhart (1953) for pure liquid. We shall follow that derivation closely here. As shown by these investigators the acoustics equations permit three waves: a thermal wave, a shear or rotational wave, and a compressional wave. The last one is the most significant as far as the attenuation of a plane acoustic wave is concerned. The other waves are important in determining the disturbance produced by a test particle in the suspension as we shall see in the next subsection.

We decompose the average velocity amplitude in scalar and vector potentials, given by

$$\langle \boldsymbol{u} \rangle = -\nabla \Phi + \nabla \times \boldsymbol{A}. \tag{35}$$

Since the curl of a gradient of any scalar function is zero, $\boldsymbol{A}$ can be specified to within a gradient of an arbitrary scalar function. To remove this arbitrariness an additional restriction is imposed that $\boldsymbol{A}$ be divergence free, i.e. $\nabla \cdot \boldsymbol{A} = 0$. It may be noted that the vorticity amplitude equals $-\nabla^2 \boldsymbol{A}$.

Introducing the decomposition in the momentum equation for the suspension (18), and rearranging, we obtain

$$\nabla \left[\mathrm{i}\omega \rho_{m,e} \Phi + \left\{ \frac{\langle c^2 \rho \gamma^{-1} \rangle_e}{-\mathrm{i}\omega} + \mu_{v,e} + \tfrac{4}{3}\mu_e \right\} \nabla^2 \Phi + \frac{1}{T} \left\langle \rho(\gamma - 1) C_v \beta^{-1} \right\rangle_e \langle T' \rangle \right]$$
$$= \nabla \times \left[\mathrm{i}\omega \rho_{m,e} \boldsymbol{A} - \mu_e \nabla \times (\nabla \times \boldsymbol{A}) \right]. \tag{36}$$

Here, we have used the vector identity $\nabla^2 \boldsymbol{a} = \nabla(\nabla \cdot \boldsymbol{a}) - \nabla \times (\nabla \times \boldsymbol{a})$. The energy equation (30) becomes

$$-\mathrm{i}\omega \langle \rho C_v \rangle_e \langle T' \rangle = \kappa_e \nabla^2 \langle T' \rangle + \left\langle \rho C_v \beta^{-1} (\gamma - 1) \right\rangle_{e,e} \nabla^2 \Phi. \tag{37}$$

Both sides of (36) must vanish separately because a rotational vector field cannot balance an irrotational field. Hence the right-hand side being zero gives, after using the above-mentioned vector identity and $\nabla \cdot \boldsymbol{A} = 0$,

$$\nabla^2 \boldsymbol{A} + k_{se}^2 \boldsymbol{A} = \boldsymbol{0} \tag{38}$$

with $k_{se}^2 \equiv \mathrm{i}\omega \rho_{m,e}/\mu_e$; k_{se} is the effective wavenumber for shear waves through the suspension.

The left-hand side of (36) being zero gives an expression for $\langle T' \rangle$ in terms of the velocity potential:

$$\langle T' \rangle = T \left[-\mathrm{i}\omega \rho_{m,e} \Phi - \left\{ \frac{\mathrm{i}}{\omega} \langle c^2 \rho \gamma^{-1} \rangle_e + \left(\mu_{v,e} + \tfrac{4}{3}\mu_e \right) \right\} \nabla^2 \Phi \right] \Big/ \left\langle \rho(\gamma - 1) C_v \beta^{-1} \right\rangle_{m,e}. \tag{39}$$

Eliminating $\langle T' \rangle$ from the energy equation for the suspension (37) by substituting for $\langle T' \rangle$ from the above yields

$$\Phi + (E - F + G) \nabla^2 \Phi - EF \nabla^4 \Phi = 0, \tag{40}$$

with

$$E = \frac{\langle c^2 \rho \gamma^{-1} \rangle_e}{\rho_{m,e} \omega^2} - \frac{\mathrm{i}}{\rho_{m,e} \omega} \left(\mu_{v,e} + \tfrac{4}{3}\mu_e \right), \tag{41}$$

$$F = \frac{\mathrm{i}\kappa_e}{\omega \langle \rho C_v \rangle_e}, \tag{42}$$

$$G = \frac{\langle \rho C_v \beta^{-1}(\gamma - 1) \rangle_{e,e} \langle \rho(\gamma - 1) C_v \beta^{-1} \rangle_{m,e}}{T \rho_{m,e} \omega^2 \langle \rho C_v \rangle_e}. \tag{43}$$

Equation (40) can be written in the form

$$\left(k_{ce}^{-2}\nabla^2 + 1\right)\left(k_{te}^{-2}\nabla^2 + 1\right)\Phi = 0, \tag{44}$$

so that $\Phi = \Phi_c + \Phi_t$ with

$$\left(\nabla^2 + k_{ce}^2\right)\Phi_c = 0, \tag{45}$$

$$\left(\nabla^2 + k_{te}^2\right)\Phi_t = 0. \tag{46}$$

The effective wavenumbers for the compressional and thermal waves are given by, respectively,

$$k_{ce}^{-2} = \tfrac{1}{2}(E - F + G) + \tfrac{1}{2}\left\{(E - F + G)^2 + 4EF\right\}^{1/2}, \tag{47}$$

$$k_{te}^{-2} = \tfrac{1}{2}(E - F + G) - \tfrac{1}{2}\left\{(E - F + G)^2 + 4EF\right\}^{1/2}. \tag{48}$$

As mentioned earlier the compressional wavenumber is the most important one as far as the acoustic wave propagation of the plane wave is concerned. The imaginary part of k_{ce} gives the attenuation while ω divided by the real part of k_{ce} gives the phase speed.

For future reference we note that the expression (39) for $\langle T' \rangle$ now can be written as

$$\langle T' \rangle = b_{ce}\Phi_c + b_{te}\Phi_t \tag{49}$$

with

$$b_{ce} = T\left[-\mathrm{i}\omega\rho_{m,e} + \left\{\frac{i}{\omega}\langle c^2 \rho \gamma^{-1}\rangle_e + \left(\mu_{v,e} + \tfrac{4}{3}\mu_e\right)\right\}k_{ce}^2\right] \Big/ \langle \rho(\gamma - 1) C_v \beta^{-1} \rangle_{m,e}. \tag{50}$$

The expression for b_{te} is similar with k_{ce} in the above replaced by k_{te}.

2.4. *An effective-medium model*

To determine the attenuation and phase speed we must now estimate various effective properties of the suspensions. This requires determining five coefficients: λ_ρ, λ_v, λ_T, λ_d, and λ_κ. Let us begin with the evaluation of λ_ρ which represents the ratio of average dilatation amplitude inside the particles to that in the suspension. This is defined by (11), which is equivalent to

$$\phi\lambda_\rho \nabla \cdot \langle \boldsymbol{u} \rangle(\boldsymbol{x}) = \int_{|\boldsymbol{x} - \boldsymbol{x}_1| \leqslant a} \langle \nabla \cdot \boldsymbol{u}_p \rangle (\boldsymbol{x}|\boldsymbol{x}_1) P(\boldsymbol{x}_1) \mathrm{d}V(\boldsymbol{x}_1). \tag{51}$$

Here, we have introduced a conditionally averaged field. Thus, $\langle \boldsymbol{u} \rangle(\boldsymbol{x}|\boldsymbol{x}_1)$ is the ensemble-averaged velocity amplitude at point $\boldsymbol{x}$ given a particle centred at $\boldsymbol{x}_1$. $P(\boldsymbol{x}_1)$ is the probability density for finding a particle with its centre in the vicinity of $\boldsymbol{x}_1$. For uniform, monodisperse suspensions $P(\boldsymbol{x}_1) = n = 3\phi/(4\pi a^3)$, n being the number density of the particles and ϕ the particle volume fraction.

We shall use an effective-medium approximation for determining the conditionally averaged fields, and hence, the integrals such as the one appearing on the right-hand side of (51). All effective-medium approximations must satisfy the criterion that far from the test particle, i.e. for $|\boldsymbol{x} - \boldsymbol{x}_1| \to \infty$, the conditionally averaged fields such as $\langle \boldsymbol{u} \rangle(\boldsymbol{x}|\boldsymbol{x}_1)$ must approach the corresponding unconditionally averaged fields such as $\langle \boldsymbol{u} \rangle(\boldsymbol{x})$. On the other hand, for $|\boldsymbol{x} - \boldsymbol{x}_1| \leqslant a$, i.e. for a point inside the test particle, the conditionally averaged fields must satisfy the equations governing the particle

phase. The simplest kind of effective medium approximation then assumes that the conditionally averaged equation satisfies the suspending fluid equations for $a \leqslant r \leqslant R$ and the unconditionally averaged equations for the suspension for $r \geqslant R$. Here, $r \equiv |\boldsymbol{x} - \boldsymbol{x}_1|$ is the distance from the centre of the particle. Different effective-medium approximations differ in their choice of R. Some investigators choose $R = a$ which eliminates the fluid region altogether. This makes the subsequent analysis very simple but, unfortunately, the estimates obtained with $R = a$ are typically inferior, and in some cases unphysical. For example, it may yield negative effective properties at high volume fractions. Other investigators choose $R = a\phi^{-1/3}$ with the incorrect reasoning that the volumes occupied by the particle and fluid for $r \leqslant R$ must be proportional to the volume fractions of the two phases. In the present study we shall choose R to be given by

$$\frac{R}{a} = \left(\frac{1 - S(\mathbf{0})}{\phi}\right)^{1/3}, \tag{52}$$

with $S(\mathbf{0})$ the zero-wavenumber limit of the suspension structure factor defined by

$$S(\mathbf{0}) = \int \left[P(\boldsymbol{r}|\mathbf{0}) - P(\mathbf{0})\right] \mathrm{d}\boldsymbol{r}, \tag{53}$$

where $P(\boldsymbol{r}|\mathbf{0})$ is the probability density for finding a particle with its centre near $\boldsymbol{r}$ given that there is a particle with its centre at origin. Note that $P(\boldsymbol{r}|\mathbf{0}) = \delta(\boldsymbol{r})$ for $r < 2a$. The above choice of R is such that

$$\int_{r \geqslant 2a} [P(\boldsymbol{r}|\mathbf{0}) - P(\mathbf{0})] \mathrm{d}\boldsymbol{r} = \int_{R \leqslant r \leqslant 2a} P(\mathbf{0}) \mathrm{d}\boldsymbol{r}. \tag{54}$$

In other words, the excess particle density outside the exclusion region in a suspension is distributed over a distance r ranging from R to $2a$ in the effective medium.

The structure factor of the suspension can be determined experimentally by a light-scattering technique but in the absence of such information one may choose $S(\mathbf{0})$ to correspond to that of a hard-sphere molecular system for which the well-known Carnahan–Starling approximation yields quite accurate estimates of the structure factor as a function of the volume fraction:

$$S(\mathbf{0}) = \frac{(1 - \phi)^4}{1 + 4\phi + 4\phi^2 - 4\phi^3 + \phi^4}. \tag{55}$$

The effective-medium radius R based on $S(\mathbf{0})$ was first introduced by Dodd *et al.* (1995) who compared the results of rigorous multiparticle interactions for determining the short-time self- and gradient-diffusivity of proteins in bilipid membranes with those obtained by the effective-medium approximation and found a very good agreement between the two. In the problems concerned with determining the collective mobility or the sedimentation velocity, where each particle is acted upon with a constant force, it was shown in Mo & Sangani (1994) that the conditionally averaged velocity has the correct leading-order behaviour at large r only when R is chosen according to (52).

For small volume fractions, $S(\mathbf{0})$ given by (55) behaves as $1 - 8\phi + O(\phi^2)$, and $R \to 2a$. Thus, in 'well-stirred' dilute random suspensions the effective medium begins at $r = 2a$ according to (52) and the fluid region $a < r < 2a$ corresponds to the excluded-volume region. Note that the more usual choice $R = a\phi^{-1/3}$ would, on the other hand, suggest that the effective medium begins at a very large distance from the test particle in a dilute suspension, which is unphysical except for the situations such

as dilute periodic or 'well-separated' random suspensions defined by Jeffrey (1973) (For such arrays $S(\mathbf{0})$ is small when ϕ is small and (52) also gives $R/a = O(\phi^{-1/3})$.) Thus it is not surprising that R based on (52) will give better estimates of the effective properites at small to moderate volume fractions compared to those obtained with $R = a\phi^{-1/3}$. Indeed, Sangani & Mo (1997) have shown that the coefficients of $O(\phi^2)$ corrections to the effective conductivity and elasticity obtained using (52) are much closer to the rigorous results for these coefficients obtained by detailed pair interaction calculations than those obtained with $R = a\phi^{-1/3}$.

Before we close this brief review of effective-medium approximations, we should perhaps note here one more class of effective-medium approximations made in the literature. These involve immersing a pair of particles in the effective medium. Examples are the calculations by Kim & Russel (1985) who estimated the permeability of a fixed bed of particles and Ju & Chen (1994)'s calculations for the effective viscosity and elasticity of suspensions with a hard-sphere spatial distribution. These calculations generally require far greater effort – comparable to direct multiparticle calculations – and do not necessarily yield superior estimates compared with the simple approximations based on a single particle. On the other hand, the single-particle approximations will be inadequate for the suspension problems in which the changes in microstructure due to imposed flow and their effects in turn on the suspension properties must be addressed.

Returning now to the problem of estimating the coefficients λ_ρ etc. using the effective-medium model consisting of a particle–fluid assembly of radius R immersed in a medium with the effective properties of the suspension, we write the velocity inside the test particle in terms of scalar and vector potentials as in the previous subsection. For the plane wave travelling along the x_1-axis with $\langle \boldsymbol{u} \rangle(\boldsymbol{x}) = -\mathrm{i}\boldsymbol{k}_{ce} \exp(\mathrm{i}\boldsymbol{k}_{ce} \cdot \boldsymbol{x})$ we have, for $|\boldsymbol{x} - \boldsymbol{x}_1| \leqslant a$,

$$\Phi_{cp}(\boldsymbol{x}|\boldsymbol{x}_1) = \exp(\mathrm{i}\boldsymbol{k}_{ce} \cdot \boldsymbol{x}_1) \sum_{n=0}^{\infty} \mathrm{i}^n (2n+1) A_{pn} P_n(\mu) j_n(k_{cp} r), \tag{56}$$

$$\Phi_{tp}(\boldsymbol{x}|\boldsymbol{x}_1) = \exp(\mathrm{i}\boldsymbol{k}_{ce} \cdot \boldsymbol{x}_1) \sum_{n=0}^{\infty} \mathrm{i}^n (2n+1) B_{pn} P_n(\mu) j_n(k_{tp} r), \tag{57}$$

$$A_p(\boldsymbol{x}|\boldsymbol{x}_1) = \exp(\mathrm{i}\boldsymbol{k}_{ce} \cdot \boldsymbol{x}_1) \sum_{n=0}^{\infty} \mathrm{i}^n (2n+1) C_{pn} P_n^1(\mu) j_n(k_{sp} r), \tag{58}$$

where $r = |\boldsymbol{x} - \boldsymbol{x}_1|$, $\mu = \cos\theta$, θ being the angle between $\boldsymbol{x} - \boldsymbol{x}_1$ and $\boldsymbol{k}_{ce}$, j_n is the spherical Bessel function of both the first kind (regular at $r = 0$), P_n is the Legendre polynomial of degree n, and P_n^1 is the associated Legendre polynomial of degree n and order 1. A_p is the only non-zero (azimuthal) component of $\boldsymbol{A}$.

Similar expressions can be written for $a < r < R$ for which the relevant wavenumbers in the expressions for Φ_{cl}, Φ_{tl}, A_l are, respectively, k_{cl}, k_{tl}, and k_{sl}. The spherical harmonics of both the first kind and second kind (corresponding to waves emanating from $r = 0$) must be included in the expression. This leads to a set of six unknowns for each mode n describing the motion in the liquid shell. Finally, for $r > R$, the potentials consist of the plane wave corresponding to the unconditional motion plus outgoing waves with wavenumbers k_{ce}, k_{te}, and k_{se}. Thus, a total of 12 unknowns are needed in describing the motion for each mode n. These are determined from the boundary conditions of continuity of velocity, traction, temperature, and heat flux amplitudes at $r = a$ and $r = R$. Note that the conditional density and temperature amplitudes can

be determined from the expressions for Φ_c, Φ_t, and A using the expressions given in the previous subsection. We keep a total of N modes (typical calculation used $N = 5$) and solve the resulting $12N$ equations numerically.

We return now to the calculation of λ_ρ. We use $\nabla \cdot \boldsymbol{u}_p = -\nabla^2 \Phi_p = k_{cp}^2 \Phi_{cp} + k_{tp}^2 \Phi_{tp}$ to convert the integral in (51) to integrals over Φ_p. Let us introduce a coefficient η_c given by

$$\phi \eta_c \Phi_c(\boldsymbol{x}) \equiv \int_{|\boldsymbol{x}-\boldsymbol{x}_1| \leqslant a} \Phi_{cp}(\boldsymbol{x}|\boldsymbol{x}_1) P(\boldsymbol{x}_1) \mathrm{d}V(\boldsymbol{x}_1). \tag{59}$$

Similarly, a coefficient η_t is introduced with $\Phi_{cp}(\boldsymbol{x}|\boldsymbol{x}_1)$ in the above replaced by $\Phi_{tp}(\boldsymbol{x}|\boldsymbol{x}_1)$. The coefficient λ_ρ is related to these two coefficients by

$$z_{ce}^2 \lambda_\rho = z_{cp}^2 \eta_c + z_{tp}^2 \eta_p. \tag{60}$$

The integration in (59) must be carried out over all $\boldsymbol{x}_1$ such that $|\boldsymbol{x} - \boldsymbol{x}_1| \leqslant a$. To convert this to an integration over $\boldsymbol{r}$ we use the identity

$$\begin{aligned} \exp\left[\mathrm{i}\boldsymbol{k}_{ce} \cdot \boldsymbol{x}_1\right] &= \exp\left[\mathrm{i}\boldsymbol{k}_{ce} \cdot \boldsymbol{x}\right] \exp\left[-\mathrm{i}r k_{ce}\mu\right] \\ &= \exp\left[\mathrm{i}\boldsymbol{k}_{ce} \cdot \boldsymbol{x}\right] \sum_{m=0}^{\infty} \mathrm{i}^m (-1)^m (2m+1) j_m(k_{ce} r) P_m(\mu). \end{aligned} \tag{61}$$

Now using $P(\boldsymbol{x}_1) = n$, substituting for Φ_{cp} from (56) into (59), making use of the above identity, and carrying out the integration, we obtain

$$\eta_c = \frac{3}{z_{ce}^2 - z_{cp}^2} \sum_{n=0}^{\infty} (2n+1) A_{pn} \left[z_{cp} j_{n-1}(z_{cp}) j_n(z_{ce}) - z_{ce} j_n(z_{cp}) j_{n-1}(z_{ce}) \right], \tag{62}$$

where $z_{cp} = k_{cp} a$ and $z_{ce} = k_{ce} a$. In the above expression j_{-1} should be taken to be $\cos(z)/z$. In deriving the above expression use has been made of the identity (Gradshteyn & Ryzhik 1994 – note that there is a sign error in their 5.54(1))

$$\begin{aligned} \int r^2 j_n(\alpha r) j_n(\beta r) \mathrm{d}r &= \frac{\pi}{2(\alpha\beta)^{1/2}} \int r J_{n+1/2}(\alpha r) J_{n+1/2}(\beta r) \mathrm{d}r \\ &= \frac{\beta r^2 j_n(\alpha r) j_{n-1}(\beta r) - \alpha r^2 j_{n-1}(\alpha r) j_n(\beta r)}{\alpha^2 - \beta^2} \end{aligned} \tag{63}$$

(recall that $j_n(z) = (\pi/2z)^{1/2} J_{n+1/2}(z)$).

The expression for η_t is similar to (61) with A_{pn} in that expression replaced by B_{pn} and z_{cp} by z_{tp}. Now λ_ρ can be evaluated by substituting for η_c and η_t in (60).

The coefficient λ_T, which represents the ratio of average temperature amplitude inside the test particle to that in the suspension, is also related to η_c and η_t. Inside the particle the temperature amplitude is a linear combination of the potentials as given by $\langle T_p' \rangle(\boldsymbol{x}|\boldsymbol{x}_1) = b_{cp} \Phi_{cp} + b_{tp} \Phi_{tp}$, where b_{cp} and b_{tp} are given by expressions similar to that for b_{ce} given earlier (cf. (50)). Now, since the unconditionally averaged thermal potential, $\Phi_t(\boldsymbol{x})$, is zero, the average temperature amplitude is given by $\langle T' \rangle(\boldsymbol{x}) = b_{ce} \Phi_c$, and therefore

$$\lambda_T = \left(b_{cp}/b_{ce}\right) \eta_c + \left(b_{tp}/b_{ce}\right) \eta_t. \tag{64}$$

The other λ coefficients can be evaluated in a similar manner and are interconnected. To determine λ_v, we need to calculate the average of the x_1-component of the velocity amplitude inside the test particle at $\boldsymbol{x}_1$. Decomposing this velocity into

three parts corresponding to contributions from the three potentials, we write

$$\lambda_v = \lambda_v^{\Phi_c} + \lambda_v^{\Phi_t} + \lambda_v^{\boldsymbol{A}}, \tag{65}$$

where λ_v^{Φ} and $\lambda_v^{\boldsymbol{A}}$ are the irrotational and rotational field contributions, respectively. It can be shown that

$$\lambda_v^{\Phi_c} = \eta_c + \frac{3}{z_{ce}} \sum_{n=0}^{\infty} A_{pn} j_n(z_{cp}) \left[n j_{n-1}(z_{ce}) - (n+1) j_{n+1}(z_{cp}) \right]. \tag{66}$$

The expression for $\lambda_v^{\Phi_t}$ is similar with η_c, z_{cp}, and A_{pn} in the above expression replaced by, respectively, η_t, z_{tp}, and B_{pn}. In deriving (66) use has been made of (61) and

$$\exp\left[-\mathrm{i}\boldsymbol{k}_{ce} \cdot \boldsymbol{r}\right] \nabla_{\boldsymbol{r}} \Phi(\boldsymbol{r}) = \nabla_{\boldsymbol{r}} \left\{ \exp\left[-\mathrm{i}\boldsymbol{k}_{ce} \cdot \boldsymbol{r}\right] \Phi(\boldsymbol{r}) \right\} + \mathrm{i}\boldsymbol{k}_{ce} \exp\left[-\mathrm{i}\boldsymbol{k}_{ce} \cdot \boldsymbol{r}\right] \Phi(\boldsymbol{r}), \tag{67}$$

with $\boldsymbol{r} = \boldsymbol{x} - \boldsymbol{x}_1$. The divergence theorem is used to evaluate the integral of the first term on the right-hand side of (67); the second term on the right-hand side is related to η_c in (66).

To evaluate the rotational contribution to λ_v we use the identity

$$\exp\left[-\mathrm{i}\boldsymbol{k}_{ce} \cdot \boldsymbol{r}\right] \nabla_{\boldsymbol{r}} \times \boldsymbol{A}(\boldsymbol{r}) = \nabla_{\boldsymbol{r}} \times \left\{ \exp\left[-\mathrm{i}\boldsymbol{k}_{ce} \cdot \mathbf{r}\right] \boldsymbol{A}(\boldsymbol{r}) \right\} + \exp\left[-\mathrm{i}\boldsymbol{k}_{ce} \cdot \boldsymbol{r}\right] \mathrm{i}\boldsymbol{k}_{ce} \times \boldsymbol{A}(\boldsymbol{r}). \tag{68}$$

The last term on the right-hand side of the above expression does not contribute to the x_1-component of the velocity, and the contribution from the first term can be readily evaluated to give

$$\lambda_v^{\boldsymbol{A}} = \frac{3}{z_{ce}} \sum_{n=1}^{\infty} n(n+1) C_{pn} j_n(z_{sp}) \left[j_{n+1}(z_{ce}) + j_{n-1}(z_{ce}) \right]. \tag{69}$$

The result for λ_v can be used to determine other λ coefficients as well. Thus, it can be shown that

$$\lambda_\kappa = \left(b_{cp}/b_{ce} \right) \lambda_v^{\Phi_c} + \left(b_{tp}/b_{ce} \right) \lambda_v^{\Phi_t}. \tag{70}$$

Finally, λ_d, defined by (27), is written as

$$\lambda_d = \lambda_v + \lambda_d^{\Phi_c} + \lambda_d^{\Phi_t} + \lambda_d^{\boldsymbol{A}}, \tag{71}$$

where we again made use of (67), with Φ replaced by $\boldsymbol{u}$. The result for $\lambda_d^{\Phi_c}$ is

$$\begin{aligned} \lambda_d^{\Phi_c} = \frac{3}{z_{ce}^2} \sum_{n=0}^{\infty} A_{pn} \Bigg[& \left\{ z_{cp} j_n'(z_{cp}) + (n+1) j_n(z_{cp}) \right\} \left\{ \left(\frac{(n+1)^2}{2n+3} + \frac{n^2}{2n-1} \right) j_n(z_{ce}) \right. \\ & \left. - \frac{(n+1)(n+2)}{2n+3} j_{n+2}(z_{ce}) - \frac{n(n-1)}{2n-1} j_{n-2}(z_{ce}) \right\} \\ & + \frac{(n+1)(2n+1)}{2n+3} j_n(z_{cp}) \left\{ (n+2) j_{n+2}(z_{ce}) - (n+1) j_n(z_{ce}) \right\} \Bigg]. \end{aligned} \tag{72}$$

An expression for $\lambda_d^{\Phi_t}$ is obtained from $\lambda_d^{\Phi_c}$ by replacing A_{pn} by B_{pn} and z_{cp} by z_{tp}. The contribution from $\boldsymbol{A}$ is given by

$$\lambda_d^{\boldsymbol{A}} = \frac{3}{z_{ce}^2} \sum_{n=1}^{\infty} (n+1) C_{pn} \left[-\frac{n(n+2)}{2n+3} X_{n,n+2} - \frac{n(2n+1)}{(2n+3)(2n-1)} X_{n,n} + \frac{n(n-1)}{2n-1} X_{n,n-2} \right] \tag{73}$$

	Polystyrene	Glass	Water	Glycerol/water
Density ($g\,cm^{-3}$)	1.055	2.3	1.0	1.08
Thermal conductivity ($J\,K^{-1}\,m\,s$)	1.15×10^{-1}	9.6×10^{-1}	5.87×10^{-1}	4.5×10^{-1}
Specific heat ($J\,g^{-1}K$)	1.19	0.836	4.19	4.19
Thermal expansion coefficient (K^{-1})	2.04×10^{-4}	3.2×10^{-6}	2.04×10^{-4}	3.22×10^{-4}
Sound speed ($cm\,s^{-1}$)	2.3×10^{5}	5.2×10^{5}	1.48×10^{5}	1.6×10^{5}
Shear viscosity ($g\,cm^{-1}\,s^{2}$)	—	—	1.01×10^{-2}	$3 \times 2 \times 10^{-2}$
Bulk viscosity ($g\,cm^{-1}\,s^{2}$)	—	—	3×10^{-2}	9.6×10^{-2}
Shear rigidity ($g\,cm^{-1}\,s^{2}$)	1.27×10^{10}	2.8×10^{11}	—	—

TABLE 1. The values of the physical properties used in the present study.

with the short-hand notation

$$X_{n,m} \equiv -\tfrac{3}{2} j_n(z_{sp}) j_m(z_{ce}) - \tfrac{1}{2}\left[z_{sp} j_n'(z_{sp}) j_m(z_{ce}) + z_{ce} j_n(z_{sp}) j_m'(z_{ce})\right]. \tag{74}$$

The scheme for estimating various effective properties and attenuation is as follows: (i) Assume initially that the effective properties of the suspension are the same as that of pure liquid. (ii) Determine the coefficients A_{pn}, B_{pn}, etc. by solving the twelve equations resulting from the application of boundary conditions at $r = a$ and $r = R$ for each mode n up to $n = 5$. (iii) Estimate λ_ρ, λ_κ, λ_v, etc. using the expressions given in this section. (iv) Estimate the effective properties of the suspension. (v) Repeat steps (ii)–(iv) until all the effective properties have converged to within a specified limit. The attenuation of the wave is given by the imaginary part of k_{ce}.

3. Comparison with known analytical results

We shall assess the effective-medium approximation in two steps. In the first, we consider various limiting situations where we expect some of the effective properties to be dominated by multiparticle interactions in Stokes or Laplace fields for which rigorous results have been obtained in recent years through direct numerical solution of the multiparticle system with hard-sphere spatial configurations. The second step will be to compare the theory with the experimental data available in the literature and some new data generated in our laboratory. This will be done in § 5.

As we have seen the acoustic problem has many variables. This makes it meaningless to present results in terms of one or two non-dimensional numbers. We shall instead choose a particular solid–liquid system and then vary either the radius of the particle or the frequency. The relevant physical properties for glass–water and polystyrene–water systems to be considered in the present study are given in table 1. In some calculations we shall vary the thermal conductivity or density of the particles without varying other physical properties to explore the effect of these properties. In some limiting cases it may be possible to solve a simplified set of equations instead of the $12N$ set of equations required by our scheme. However, since our primary purpose is to assess the effective-medium approximation and the computer program written for this purpose we use the same program in all the comparisons shown here.

The effective viscosity of the suspension will be in general complex with the imaginary part multiplied by frequency being the elasticity of the suspension. Results of rigorous multiparticle computations are available in the literature for the case when inertia is negligible (Stokes flow) and a uniform strain rate is applied to suspensions of rigid particles in an incompressible, Newtonian fluid. The spatial distribution

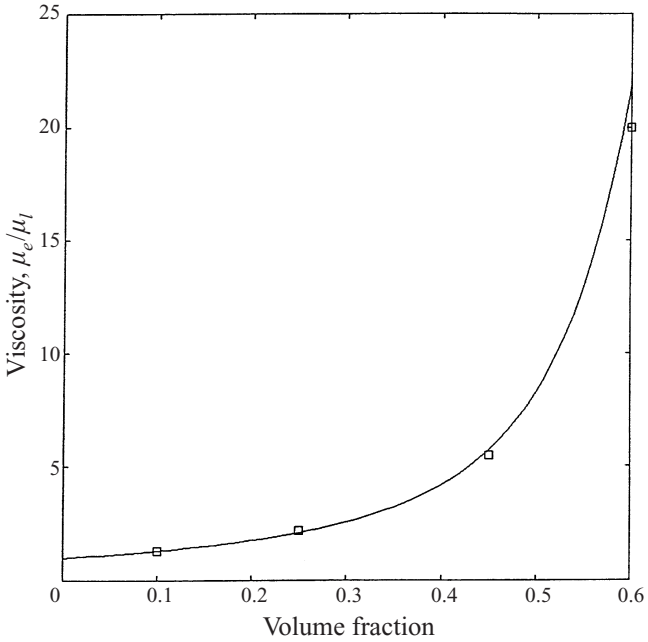

FIGURE 1. Ratio of effective viscosity to liquid viscosity as a function of volume fraction. Limiting values for wavelengths large compared to particle size and viscous boundary layers much larger than the particles. Solid line is theory; squares are numerical simulation results from Sangani & Mo (1997).

of the particles corresponded to the hard-sphere molecular systems for which $S(\mathbf{0})$ given by (55) applies. Ladd (1990) obtained the results with volume fractions (ϕ) in the range 0–0.45. Mo & Sangani (1994) and Sangani & Mo (1997) repeated and confirmed his results and also obtained an additional result for $\phi = 0.6$. Their results are shown in figure 1. To see how well the effective-medium model developed in the present study approximates these values we must pick frequencies for which the quasi-steady Stokes flow approximation will be expected. The ratio of unsteady to viscous terms in the momentum equation for the liquid is $\rho_l \omega a^2/\mu_l$. For $a = 10^{-5}$ cm and $f = \omega/2\pi = 10^6$ Hz this number equals 6×10^{-3} (we have taken water as the suspending liquid but multiplied the viscosity by 10). The wave nature of the governing equations depends on the ratio $k_{cl}a$ which equals 2π times the ratio of particle radius to the wavelength in pure liquid. When this number is small the liquid may be treated as essentially incompressible. For a and f listed above, $k_{cl}a$ for water equals 4.2×10^{-4}. Finally, our calculations account for small deformations of the particles. For particles to be treated as rigid, their shear modulus $\tilde{\mu}$ divided by the frequency must be much larger than the viscosity of the water. At $\omega = 10^6/2\pi$ s^{-1}, the ratio $\tilde{\mu}/(\omega\mu_l)$ equals 2×10^7 and therefore the glass particles may be treated as rigid.

The solid curve in figure 1 represents the estimates of the effective viscosity obtained by the effective medium model for the aforementioned conditions. The ratio $\mathrm{Re}(\mu_e)/\mu_l$ varies from unity to about 20 as ϕ is varied from 0 to 0.6. At high volume fractions significant viscous dissipation occurs in the narrow gap regions between the pairs of particles in close proximity and this dominates the effective viscosity behaviour at high ϕ. This phenomenon cannot be expected to be modelled accurately by the

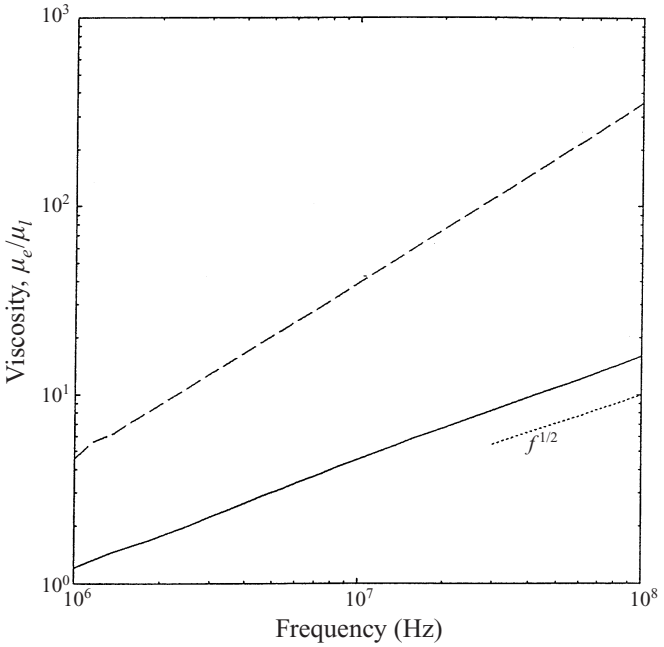

FIGURE 2. Real part minus its limiting value at large wavelengths (—) and minus imaginary part (– – –) of the ratio of effective viscosity to liquid viscosity as a function of frequency. Particle volume fraction is 0.3. The viscous boundary layers at the lowest frequencies are small compared to the particle size (at 1 MHz, $(\mu_l/(\rho_l\omega^2a^2))^{1/2} = 0.01$).

single-particle approximation used here and therefore the excellent agreement found here for $\phi = 0.45$ and 0.6 may be regarded as fortuitous. It should also be noted that the particles in highly concentrated suspensions may begin to be supported by the other particles through the formation of a continuous network such that the suspension behaves like a fluid-filled porous medium. The present analysis should not be applied to such suspensions.

Figure 2 shows that the real and imaginary parts of the effective viscosity increase with frequency in the range where the unsteady term begins to become comparable to the viscous term in the liquid momentum equation. The results for the real part of the effective viscosity may be rationalized as follows. At relatively large frequencies we expect the viscous effects to be confined to small Stokes layers of thickness $\delta = O((\mu_l/\rho_l\omega)^{1/2})$ surrounding each particle. The effective viscosity is the rate of energy dissipation per unit volume of the suspension divided by the square of mean velocity gradient $\dot{\gamma} = O(k_{ce}\langle \boldsymbol{u} \rangle)$. At high frequencies the dominant contribution to dissipation arises from the Stokes layers whose volume per unit suspension volume is $O(\delta a^2 n)$, n being the number density of particles, and the velocity gradient in these layers is $O(\dot{\gamma}a/\delta)$. The effective viscosity must therefore roughly scale as a/δ or $a(\omega\rho_l/\mu_l)^{1/2}$ for frequencies at which δ is small compared with a. The observation that the real part of effective viscosity should increase with frequency as $\omega^{1/2}$ is consistent with the results of figure 2. The ratio $(\mu_l/\rho_l\omega a^2)^{1/2}$ is about 0.01 for $f = 1$ MHz indicating that indeed the Stokes layers are thin at these frequencies (note that we have replaced μ_l by its value for water divided by 1000).

The imaginary part of the effective viscosity is also seen to increase with increasing

frequency in figure 2. This elastic nature of the suspension is expected at higher frequencies.

We now compare the effective-medium results for λ_v with the known results. Recall that λ_v represents the ratio of the velocity amplitude in the particle phase to that in the suspension. At lower frequencies for which $k_{ce}a$ is small and the scattering losses are small, the attenuation will be dominated by the imaginary part of λ_v as suggested by Sangani *et al.* (1991) who evaluated the real and imaginary parts of λ_v for a special case when the frequency is large enough for the Stokes layers to be small compared with the particle radius but small enough for $k_{ca}a$ to be small, i.e. for the suspension to be essentially incompressible. We shall compare the results of effective-medium approximation with their results next.

Sangani *et al.* gave their results in terms of added mass, Basset, and viscous drag coefficients. The force balance on a particle in the suspension was written as

$$\langle \boldsymbol{F}(t)\rangle = \rho_l \mathscr{V}\langle \dot{\boldsymbol{u}}\rangle + \tfrac{1}{2}\rho_l \mathscr{V} C_a\langle \dot{\boldsymbol{u}}-\dot{\boldsymbol{v}}\rangle + 6a^2\sqrt{\pi\rho_l\mu_l}C_b\int_{-\infty}^{t}\langle \dot{\boldsymbol{u}}-\dot{\boldsymbol{v}}\rangle(\tau)\frac{\mathrm{d}\tau}{\sqrt{t-\tau}} + 6\pi a\mu_l C_d\langle \boldsymbol{u}-\boldsymbol{v}\rangle \tag{75}$$

where $\boldsymbol{F}$ is the force on the particle, $\mathbf{v}$ is the velocity of the particle, C_a, C_b and C_d are the added mass, Basset and viscous drag coefficients and $\mathscr{V}$ the volume of a particle. Dots above variables denote time derivatives. Noting that $\boldsymbol{F}(t) = \rho_p \mathscr{V}\dot{\boldsymbol{v}}$ and $\langle \boldsymbol{v}\rangle = \lambda_v\langle \boldsymbol{u}\rangle$, and taking the time-dependence of variables to be $\mathrm{e}^{-\mathrm{i}\omega t}$, the force balance (75) gives

$$C_a + 9\Omega C_d + 9\Omega^2 C_d = \frac{2(\rho^*\lambda_v - 1)}{1-\lambda_v}, \tag{76}$$

with $\Omega \equiv (\mathrm{i}\mu_l/(\rho_l\omega a^2)^{1/2}$ and $\rho^* \equiv \rho_p/\rho_l$. Sangani *et al.*'s analysis is valid when the magnitude of Ω is small compared with unity, and the terms of $O(\Omega^3)$ or smaller are neglected in (76). For small Ω, λ_v can be expanded in a series $\lambda_v = \lambda_v^{(0)} + \Omega\lambda_v^{(1)} + \cdots$ to yield the relations

$$C_a = \frac{2(\rho^*\lambda_v^{(0)} - 1)}{1-\lambda_v^{(0)}}, \qquad C_b = \frac{2\lambda_v^{(1)}(\rho^* - 1)}{9\left(1-\lambda_v^{(0)}\right)^2}. \tag{77}$$

The coefficients $\lambda_v^{(0)}$ and $\lambda_v^{(1)}$ were evaluated from the effective-medium theory results for λ_v at small $k_{cl}a$ and small $|\Omega|$ by extrapolating to $\Omega = 0$ and numerically differentiating the results with respect to Ω, respectively. Figures 3 and 4 show a comparison with the rigorous multiparticle calculations of Sangani *et al.* who determined C_a, C_b, and C_d as a function of ϕ and ρ^* for periodic as well as random arrays of spheres. The results for C_a for the body-centred cubic and random arrays were very close to each other while that for the simple cubic arrays differed by about 12% at $\phi = 0.5$. It was also found that the dependence on ρ^* was rather weak, typically variations within 5% occurred as ρ^* was varied from zero to infinity. The results of Sangani *et al.* shown in figures 3 and 4 correspond to $\rho^* = 0$ while the effective-medium results correspond to glass particles in water with $\rho^* = 2.55$. We see an excellent agreement between the added mass coefficient obtained by the effective-medium approximation and for random or body-centred cubic arrays. The effective-medium approximation for C_b deviates systematically from the random arrays result with the maximum deviation of about 20% at $\phi = 0.5$. The theory in this case is much closer to the results for the simple cubic arrays.

Next we consider the case when Ω is very large, i.e. frequencies at which the

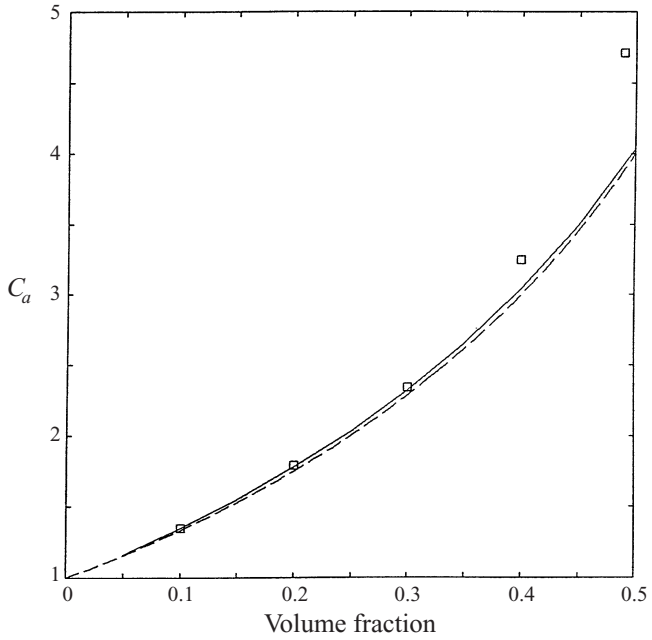

FIGURE 3. Added mass coefficient C_a as a function of volume fraction. Solid line is the theoretical result for wavelengths and viscous boundary layers much larger than particle size. Broken line and squares are the random array and simple cubic array results of Sangani *et al.* (1991). Particle to liquid density ratio is 2.55.

viscous drag coefficient makes the leading contribution to λ_v. The results in this case can be compared with the results of multiparticle Stokes flow calculations by Ladd (1990) and Mo & Sangani (1994). Two kinds of results are available in the Stokes flow literature. The first is the hindrance factor in sedimentation in which the average velocity of the particles is determined for the case when the forces acting on all the particles are the same. The second is the calculation of the permeability of a fixed bed of particles. There the average force on the particles is calculated for particles that all have the same (zero) velocity, different from the mean velocity of the suspension. Neither situation applies to oscillatory flows but one expects that the results for the fixed bed resistivity would be most applicable for large ρ^* and those of the hindrance factor for very small ρ^*. Figure 5 compares the results of Ladd and Mo & Sangani for these two quantities with the results obtained using the effective-medium approximation with $\rho^* = 10$. These results were obtained with $|\Omega| = 22$ and $k_{cl}a = 0.001$. The results for the sedimentation-hindrance factor were obtained only up to $\phi = 0.45$ in the present investigation while Mo & Sangani had obtained an additional value for the fixed bed resistivity at $\phi = 0.6$. Their result for $\phi = 0.6$ was in excellent agreement with the well-known Carman–Kozney correlation. We see that at least up to $\phi = 0.45$, the hindrance factor and the fixed-bed resistivity are not too different from each other, and that the effective-medium results are in excellent agreement for the entire range of ϕ.

Next, we compare the results for the effective conductivity. When $k_{cl}a$ is small the viscous and thermal effects contribute most to the total attenuation. When the density ratio is close to unity the translational oscillations and hence viscous attenuation are small and the thermal effects become the primary source of attenuation. The effective

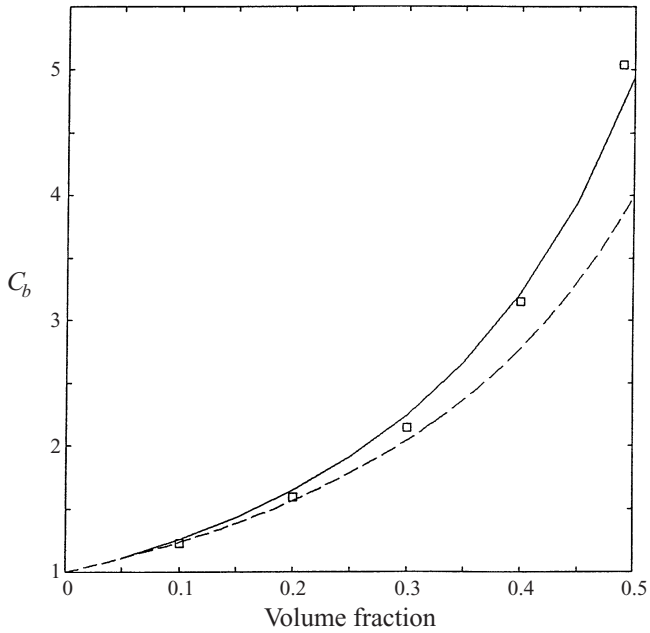

FIGURE 4. Basset coefficient C_b as a function of volume fraction. Solid line is the theoretical result for wavelengths and viscous boundary layers much larger than particle size. Broken line and squares are the random array and simple cubic array results of Sangani *et al.* (1991). Particle to liquid density ratio is 2.55.

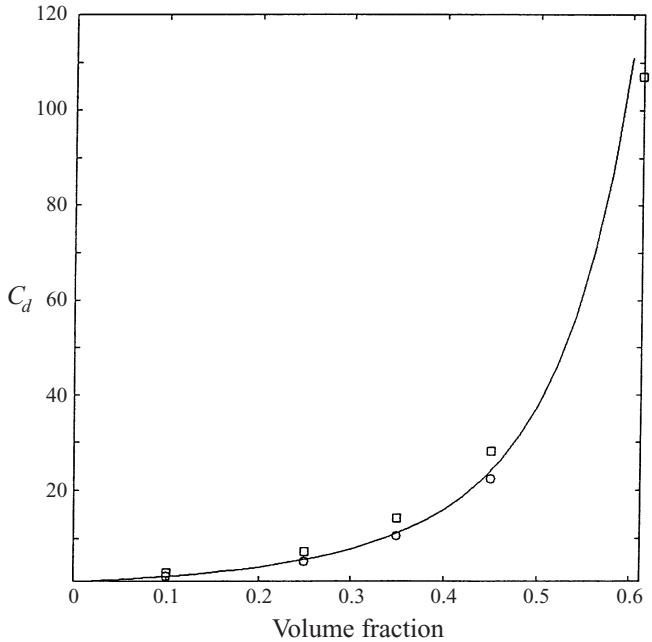

FIGURE 5. C_d as a function of volume fraction. Lines are theoretical results obtained for wavelengths much larger and viscous boundary layers much smaller than particle size. Squares are numerical simulation results for the fixed-bed resistivity by Mo & Sangani (1994), circles are numerical simulation results for the hindrance factor by Ladd (1990).

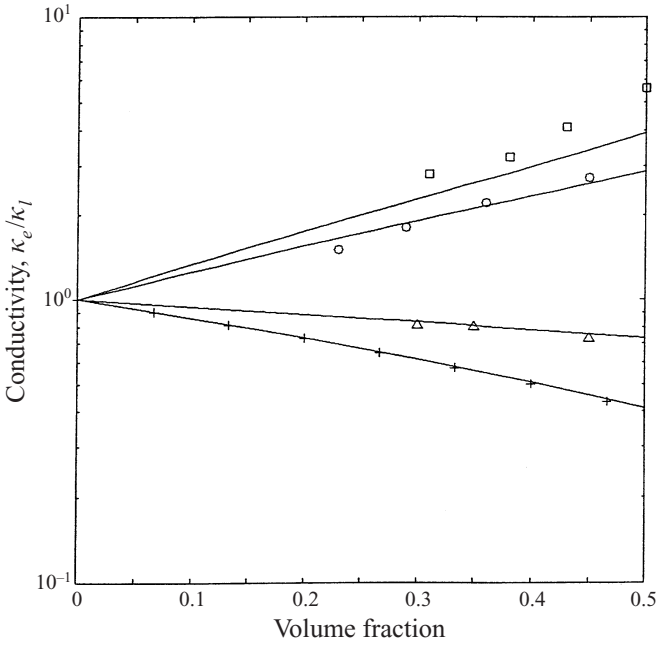

FIGURE 6. Ratio of effective conductivity to liquid conductivity as a function of volume fraction. Lines are theory for wavelengths large compared to particle size, symbols are experimental data from Turner (1976). Results are shown for $\kappa_p/\kappa_l = 0.01$ (+), 0.51 (△), 10.8 (○) and 160 (□).

conductivity as a function of ϕ and the conductivity ratio κ_p/κ_l was determined experimentally by Turner (1976) who used liquid fluidized beds of nearly monodisperse spheres. Sangani & Yao (1988) and Bonnecaze & Brady (1991) have carried out multiparticle calculations for the same cases and found generally good agreement between the simulations results and the experimental data of Turner. Figure 6 shows the comparison between the effective-medium approximation and the data of Turner. Calculations were made with the polystyrene–water system with $f = 1$ MHz for which $k_{cl}a$ equals 4.2×10^{-4} and the ratio of unsteady term to the steady conduction term $\rho_l C_{p,l}\omega a^2/k_l$ equals 0.05. The thermal conductivity of the particles was varied keeping other parameters fixed to determine the effect of conductivity ratio. Agreement is generally very good except for the highest particle-to-liquid conductivity ratio of 160 and $\phi = 0.5$ for which the effective-medium approximation underpredicts the effective conductivity by about 30%. At such high conductivity ratios the narrow gap regions between pairs of particles in dense suspensions contribute siginificantly to the overall heat flux and this is not captured accurately by the effective-medium approximation. The spatial distribution of the particles could also affect significantly the results at high ϕ. For low-conductivity particles we see an excellent agreement between the experiments and the effective-medium approximation. It may be noted that the well-known Maxwell relation

$$\frac{\kappa_e}{\kappa_l} = \frac{1 + 2\alpha\phi}{1 - \alpha\phi} \tag{78}$$

with $\alpha = (\kappa_p - \kappa_l)/(\kappa_p + 2\kappa_l)$ also gives accurate estimates of the effective conductivity for $\kappa_p/\kappa_l = 0$.

Figure 7 shows the results for the real and imaginary parts of the effective con-

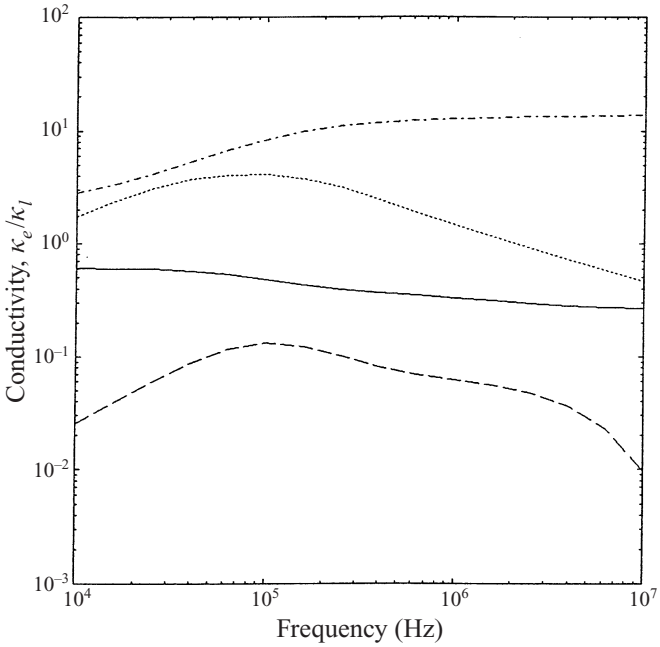

FIGURE 7. Real and imaginary part of the ratio of effective conductivity to liquid conductivity as functions of frequency. Particle volume fraction is 0.3; $k_{cl}a = 4 \times 10^{-2}$ at 10 MHz for all cases. Solid line (real part) and dashed line (imaginary part), $\kappa_p/\kappa_l = 2 \times 10^{-3}$; dashed-dotted line (real part) and dotted line (imaginary part), $\kappa_p/\kappa_l = 20$.

ductivity as a function of frequency for two particle-to-liquid conductivity ratios. For $\kappa_p/\kappa_l > 1$ the real part of the conductivity is seen to increase with the frequency. This result is similar to the one discussed for the effective viscosity (cf. figure 2). The opposite is true for the particles whose conductivity is smaller than the fluid conducitivity. The imaginary part of the conductivity is seen to reach a maximum at frequencies for which the thermal layer thickness is comparable to particle radius.

In summary, we have shown in this section that the effective-medium approximation yields very accurate estimates of the coefficients λ_d (effective viscosity), λ_v (added mass, Basset force, and viscous drag), and λ_κ (conductivity) for the monodisperse, random suspensions in the limits in which the results of exact multiparticle interactions are available.

The two coefficients for which no exact results are available are λ_ρ and λ_T but the computed results for these coefficients show expected trends. For example, figure 8 shows results for the real and imaginary parts of λ_T which represents the ratio of average temperature amplitude inside the particles to that in the suspension. The results are shown for polystyrene–water mixture with $a = 0.11\,\mu\text{m}$, a system which was studied by Allegra & Hawley (1972). When the thermal diffusion length, $(\kappa_p/\omega\rho_p C_{v,p})^{1/2}$, becomes much larger than the particle radius, the temperature inside the particle will be the same as the suspension temperature and λ_T will approach unity. This is the situation for frequencies less than 1 MHz. At frequencies that are large enough so that the thermal layer inside the particles is thin compared with the radius but small enough to keep the wavelength large compared with the radius, we expect the particle temperature amplitude to be governed by the temparature variations in the adiabatic case. A simple calculation shows that in this limit λ_T and

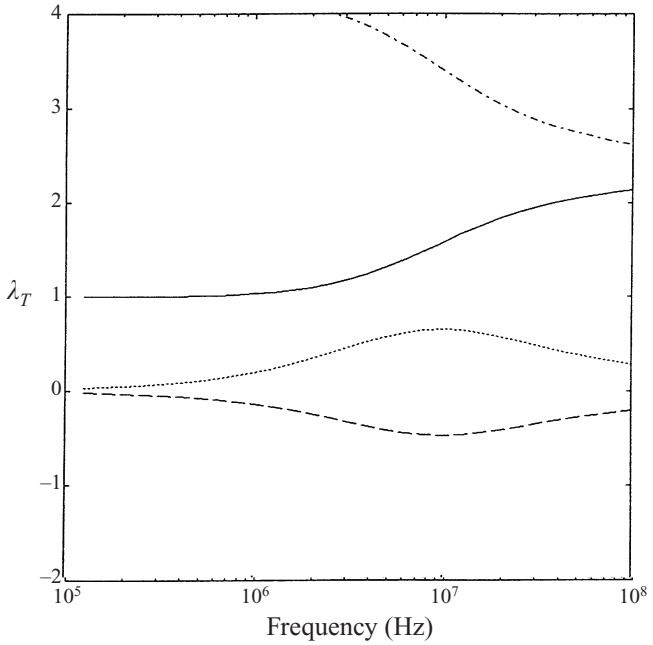

FIGURE 8. Real and imaginary parts of λ_T as a function of frequency for polystyrene particles (0.11 μm radius) in water at 0.3 volume fraction. Solid line (real part) and dashed line (imaginary part) are the full results; the dashed-dotted line (real part) and the dotted line (imaginary part) are the adiabatic result (79).

λ_ρ are related by

$$\lambda_T = \frac{(\gamma_p - 1)\lambda_\rho k_{ce}^2}{\mathrm{i}\omega b_{ce}\beta_p}. \tag{79}$$

The dot-and-dashed curve in figure 8 is obtained by first computing λ_ρ using the effective-medium approximation and then using (79) to estimate λ_T. We see that at high frequencies the result for λ_T obtained in this manner approaches that obtained from the direct evaluation using the effective-medium approximation. The imaginary part of λ_T is seen to vanish in the limits of high and low frequencies as one approaches, respectively, the adiabatic and isothermal limits.

All the results discussed in this section correspond to the limit of small $k_{cl}a$ for which the scattering losses are insignificant. Since all indications suggest that the effective-medium approximation is very accurate, we expect the theory to predict the thermal and viscous attenuations for small $k_{ce}a$ very accurately. Rigorous calculations are not available for $k_{cl}a = O(1)$ and we shall mostly depend on the experimental data to assess the effective-medium theory in this regime.

4. Experimental set-up

The experimental set-up for measuring attenuation is shown in figure 9. The suspension is hand-stirred in a vessel with transmitting and receiving transducers mounted flush with the inner walls. The distance between the transducers in a typical vessel was 5 cm, the width and the height of the vessel being 8 and 13 cm, respectively. In dense suspensions for which greater attenuation is expected, the experiments were carried out with smaller vessels with the acoustic path lengths as small as 1.3 cm.

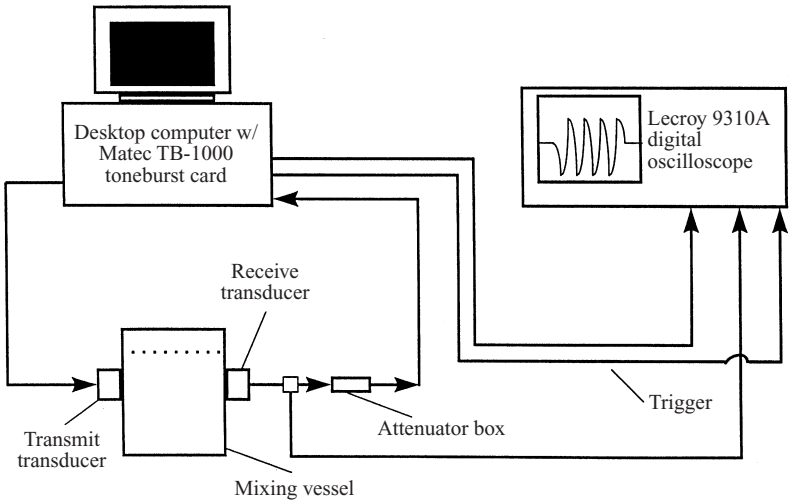

FIGURE 9. The schematic of the experimental set-up.

The transducers were of piezoelectric videoscan immersion type manufactured by Panametrics Inc. To cover a relatively broad range of frequencies, we used transducers with centre frequencies of 1.0, 2.25, 5.0, 7.5 and 10.0 MHz. The first two were 1.3 cm in radius while the other two were 1 cm in radius.

A Matec TB-1000 digital synthesizer card installed in a desk-top computer was used to generate monochromatic tonebursts that propagated through the suspension and were received by the receiving transducer. The signal was then sent to a LeCroy Model 9310A digital oscilloscope where its amplitude was measured. Attenuation data were obtained for six to eight frequencies for each transducer pair. Thus, the measurements were typically carried out at frequencies between 1 and 12 MHz. The suspension was hand-stirred before each measurement. To calculate the excess attenuation caused by the presence of particles, we also measured the amplitude of the signal received by the transducer for the pure liquid case. The excess attenuation for a given particle concentration is then determined using

$$\alpha = -\frac{1}{L}\log\left(\frac{V_{\mathrm{mix}}}{V_l}\right), \tag{80}$$

where V_{mix} and V_l are the voltage amplitudes of the received signals in the mixture and pure liquid, respectively, and L is the distance between the transducers.

Further details about the experimental set-up can be found in Norato (1999).

5. Comparison with experiments

Several experimental results have been presented for dense slurries in the literature. In this section we shall compare with these data as well as with results obtained in our laboratory. Allegra & Hawley (1972) measured attenuation for nearly monodisperse polystyrene particles of radius 0.11 μm in water. The acoustic frequency range used by these investigators was roughly 5–50 MHz. This corresponds to the non-dimensional wavenumbers $k_{cl}a$ in the range of 0.002–0.02. At such small wavenumbers the scattering losses are negligible, and since the density of polystyrene (1.07 g cm^{-3}) is close to that of water, the translational oscillations of the particles and hence the vis-

cous attenuation are negligible. Thus, the thermal effects dominate the attenuation in Allegra & Hawley's experiments. The difference in thermal expansion coefficients between the particles and the suspending liquid causes the temperature amplitude inside the particles to differ from that in the liquid. This causes a heat flux through the surface of the particles that is out of phase with the sound wave and leads to thermal attenuation.

Allegra & Hawley showed that when the thermal boundary layers as well as the wavelength are much greater than the particle radius and the suspension is dilute (i.e. when $\kappa_l/(\rho_l C_{p,l}\omega a^2) \gg 1$, $k_{cl}a \ll 1$, and $\phi \ll 1$), the attenuation is given by

$$\alpha = \tfrac{1}{6}\phi\omega^2 a^2 c_l T \rho_l \rho_p^2 C_{p,p}^2 \left(\frac{\beta_l}{\rho_l C_{p,l}} - \frac{\beta_p}{\rho_p C_{p,p}}\right)^2 \frac{1}{\kappa_p}\left[\frac{1}{5} + \frac{\kappa_p}{\kappa_l}\right]. \tag{81}$$

The attenuation increases as f^2 in this limit. On the other hand, when the boundary layers are much smaller than the particles while $k_{cl}a$ is still small, their analysis predicts that the attenuation will increase with frequency as $f^{1/2}$.

Allegra & Hawley (1972) compared their data with a theory for dilute suspensions and found good agreement between the two for dilute suspensions. Since the effective-medium theory reduces to their theory for dilute suspensions as $\phi \to 0$, we also expect a very good agreement at small volume fractions. Allegra & Hawley compared the two in several of their figures but did not specify the volume fraction of the particles used in obtaining the data except for one in which they show the attenuation as a function of ϕ at several frequencies. We show their data for the lowest volume fraction, $\phi = 0.058$, in figure 10. The asymptotic expression (81) is also shown in the figure; it is seen that the experiments were carried out at frequencies for which the thermal layers are comparable to particle radius.

As noted by Allegra & Hawley, the attenuation is sensitive to the thermal properties of polystyrene particles. If we take these properties to be the same as given by these investigators and reported in table 1, we find that the predicted attenuation is slightly greater than the experimental values as indicated by the solid line in figure 10. However, there is some uncertainty about the values of the physical properties as given by Allegra & Hawley. In their paper they show that their results depend quite strongly on the equilibrium temperature – because the physical properties do – and that there is a significant discrepancy between the theory and experiments in this temperature dependence. Especially, the attenuation at temperatures $\leqslant 20^\circ$ C is overpredicted. Allegra & Hawley mentioned that the factor $\beta_p/(\rho_p C_{p,p})$ (cf. (81)) introduces the uncertainty. To be able to have a fair comparison between the dense slurry data and the effective-medium theory we have therefore changed the value of β for polystyrene somewhat (decreased by 11%) to get the best fit at low volume fractions, which is seen to be excellent.

Figure 11 compares the effective-medium approximations with the attenuation data as a function of volume fraction of the particles at different frequencies. We see an excellent agreement at all volume fractions. (Slight differences seen are within the error introduced in reading the data from Allegra & Hawley's figures or due to small temperature variations that could occur during the experiments.) Note that simply using the dilute theory of Allegra & Hawley (1972) would have overpredicted the attenuations at 0.5 volume fraction by as much as 50%.

The scattering attenuation was small in the experiments by Allegra & Hawley (1972) since $k_{cl}a$ for their experiments was much less than unity. To extend the range of $k_{cl}a$ over which the theory can be tested against experiments we have conducted

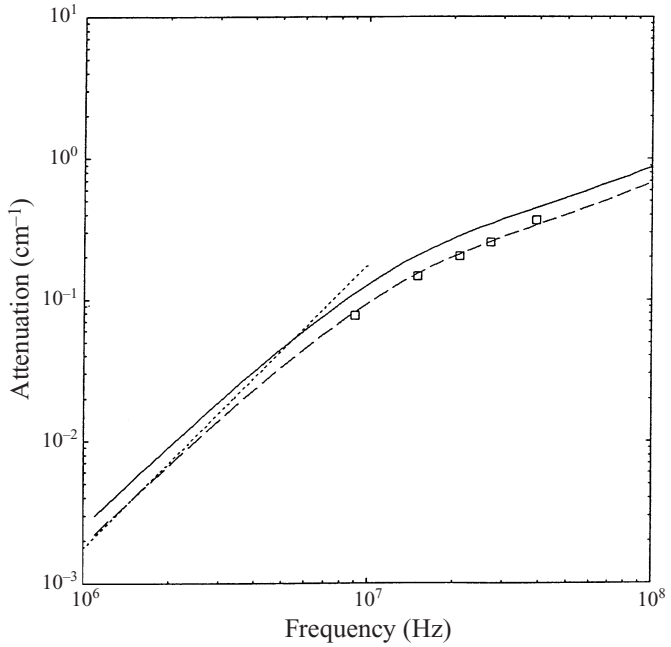

FIGURE 10. Comparison with experimental dilute-slurry results by Allegra & Hawley (1972) for the attenuation in a mixture of polystyrene particles of 0.11 μm radius in water at 0.05 volume fraction. Squares are experiments, solid line is the theoretical result. The broken line is the theoretical result when the thermal expansion coefficient is changed from 2.04×10^{-4} to $1.82 \times 10^{-4}\,\mathrm{K}^{-1}$. The dotted line is the asymptotic result (81).

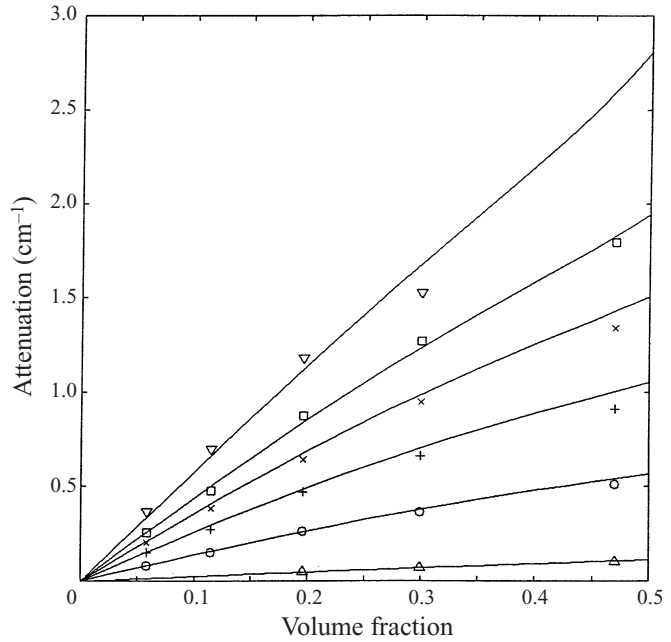

FIGURE 11. Comparison with experimental dense-slurry results by Allegra & Hawley (1972) for the attenuation for polystyrene particles of 0.11 μm at different frequencies. △, 3 MHz; ○, 9 MHz; +, 15 MHz; ×, 21 MHz; □, 27 MHz and ▽, 39 MHz.

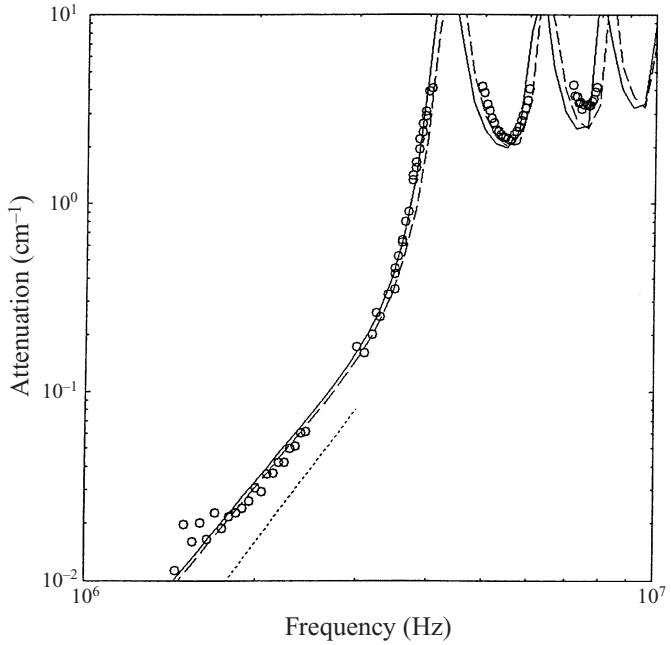

FIGURE 12. Experimental and theoretical results for the attenuation in a mixture of polystyrene particles (mean radius $79 \pm 3\,\mu$m and $1.8\,\mu$m standard deviation) in water at 0.05 volume fraction. Circles are experiments, solid and broken lines are the theory for monodisperse particles of $79\,\mu$m and $77\,\mu$m radius, respectively.

experiments for much larger polystyrene particles. The particles were specified by the manufacturer to have a mean radius of $79 \pm 3\,\mu$m with a standard deviation of $1.8\,\mu$m; $k_{cl}a$ in our experiments varied between 0.5 and 2.6. The comparison between the theory and experiments is shown in figure 12. At small frequencies (or small $k_{cl}a$) the attenuation due to scattering is expected to increase in proportion to f^4. This behaviour is observed roughly for $k_{cl}a < 1.3$. At higher frequencies the resonance effects due to various shape deformations of the particles become important as discussed in more detail by Spelt *et al.* (1999) who examined the problem of determining size distributions for dilute suspensions. The first three peaks seen in figure 12 correspond to the resonances in $n = 2,3$, and 4 modes (cf. (56)).

As we can see from figure 12, the agreement between the theory and the experiments is very good. A possible explanation for the slight differences observed near the resonance peaks is the uncertainty in the mean particle size as specified by the manufacturer. Changing the size of the particles from 79 to $77\,\mu$m radius (which is within the specifications) is seen in figure 12 to improve the comparison. Alternatively, an excellent agreement can also be observed by accounting for the size distribution of particles.

Most of the data shown in figure 12 were taken for a suspension with $\phi = 0.05$. High attenuation near the resonance peaks is not measurable and this explains the gaps seen in the data near those frequencies. We repeated some experiments with $\phi = 0.025$ and with smaller vessels which decreased the acoustic path length between the two transducers and obtained a few data points near the resonances but additional measurements with very low volume fractions appeared unnecessary.

Since the volume fraction used in this measurement is rather small ($\phi = 0.05$), an

excellent comparison between the theory and experiments should not be regarded as a true test of the effective-medium approximation. Rather, it shows that the data taken in our laboratory are reliable and that our analysis and the computer program for the effective-medium approximation gives correct results over a wide range of frequencies. To test the effective-medium theory higher volume fractions must be used but we encounter two problems. First, the monodisperse polystyrene particles in this size range are extremely expensive and secondly the range of frequencies for which the attenuation at higher volume fractions would be measurable will be rather narrow to provide a good test of the effective-medium approximation.

Experiments on dense slurries in the frequency range that is dominated by scattering effects before the resonance peaks were done by Atkinson (1991) and Atkinson & Kytömaa (1992). We have compared their data for the dilute suspensions with the present theory and found that, although the agreement at the lower half of their frequency range is reasonable, at higher frequencies the experimental results for the attenuation were consistently lower than the theoretical results (at 0.045 volume fraction and 0.7 MHz frequency the difference was a factor two). It was found that the differences could not be resolved by changing the physical properties, the size of the particles or by allowing for a size distribution of the particles. Since we do not see any reason for the theory to be inapplicable at such low volume fractions, we did not pursue further comparison at higher volume fractions. Instead, we shall compare the theory with the experiments we have conducted for the glass–water system.

Since the large glass particles are difficult to keep suspended in water, we added glycerol to increase the viscosity and density of the suspending medium. Soda-lime glass particles were used. The volume fraction size distribution was measured using a light scattering instrument and gave a mean radius of 63 μm and a standard deviation of 8.5 μm (the volume fraction distribution is related to the size distribution $P(a)$ by $\phi(a) = (4/3)\pi a^3 P(a)$). The distribution is shown in figure 13 together with a fit used in calculations discussed below (a lognormal size distribution for $P(a)$ was used). The instrument could measure the particle radius up to about 240 μm. It was estimated that about 1.5% of the particles by volume had radius that exceeded this value.

We first discuss results for a dilute suspension. Figure 14 shows the attenuation as a function of frequency at $\phi = 0.05$. At the frequency of 1 MHz, the non-dimensional wavenumber $k_{cl}a$ based on mean radius is about 0.25. Thus, throughout the frequency range we expect the scattering losses to be the most significant. At low frequencies, the attenuation is approximately proportional to f^4. Note that at very low frequencies the viscous attenuation will become more significant, and if the Stokes layers are small compared with the particle radius, then the attenuation will be proportional to $f^{1/2}$. At higher frequencies the attenuation appears to level off, unlike the case of polystyrene particles which exhibited distinct resonance peaks. This qualitative difference arises due to different shear moduli of glass and polystyrene (Spelt *et al* 1999).

The solid curve in figure 14 is obtained by using the size distribution shown in figure 13 which ignores the particles larger than 240 μm. We see that the agreement between the theory and the experiments is very good at frequencies above 2 MHz. Significant discrepancy exists, however, at lower frequencies. This may be due to the presence of larger particles. If we assume that, in addition to the size distribution shown in figure 14 we had 1.5% by volume of particles with a radius of 540 μm, then we obtain the dashed curve shown in figure 14. These larger particles contribute most to the attenuation for smaller frequencies. Alternatively, it is possible that some of the assumed physical properties of the water–glycerol system (cf. table 1) may

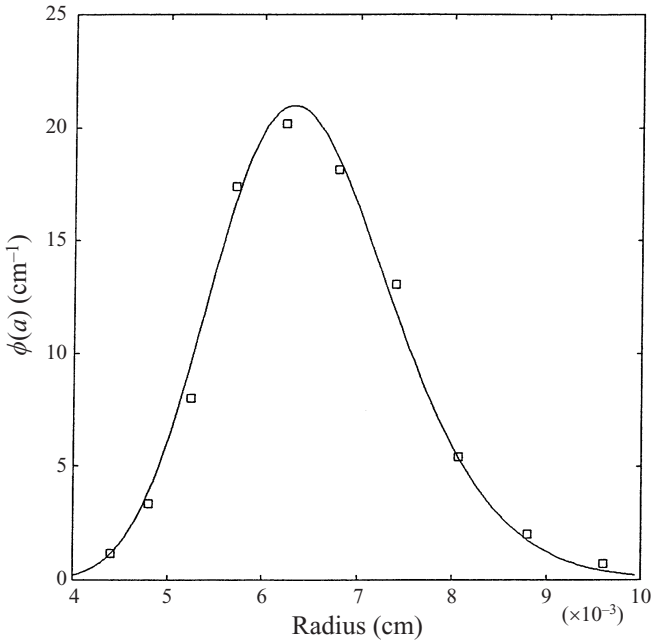

FIGURE 13. Volume-fraction distribution of the glass particles used in figure 14. Circles are measurements, the solid line is a fit using a log-normal size distribution.

be inaccurate and this may lead to the observed discrepancy at lower frequencies. The density and viscosity were measured in our laboratory but the other properties (sound speed and attenuation) were estimated using a volume-average mixture rule. In view of these uncertainties we shall only compare the experimental data for dense suspensions for frequencies greater than 2 MHz where the agreement for dilute suspensions is good.

Since the size distribution is somewhat broad, we must modify the effective-medium theory to account for polydispersity. The coefficients λ_ρ, etc. to be used in determining the effective properties of the suspension are now replaced by $\sum_{n=0}^{M} \phi(a_i)\lambda_\rho(a_i)$, etc. where M is the number of particle size bins. Here, $\lambda_\rho(a_i)$ represents the ratio of average dilatation amplitude inside the particle of radius a_i to that in the suspension. To estimate such coefficients we assume that the particle of radius a_i is surrounded by the liquid up to $r = R_i$ and the effective medium for $r > R_i$. We take R_i/a_i to be the same for all particle sizes and given by the same expression as in the case of a monodisperse suspension (cf. (52)). This is probably not a good estimate of R_i/a_i since one would expect R_i/a_i for larger particles to be smaller than for monodisperse suspensions as the volume exclusion for larger particles is smaller when smaller particles are present in the suspension. However, since there are no known analytical, rigorous solutions for polydisperse suspensions, a more complicated scheme for estimating R_i/a_i would be difficult to justify.

The dense-slurry data for the glass–water/glycerol suspensions are shown in figure 15. The frequency range is 2.5–5 MHz for which the comparison at $\phi = 0.05$ shown in figure 14 was good. The agreement is seen to be very good up to $\phi = 0.3$. At higher volume fractions, however, we observe significant discrepancy. The theory predicts the attenuation to be a monotonically increasing function of ϕ while the experiments exhibit maxima near $\phi = 0.3$. The measurements were made two or

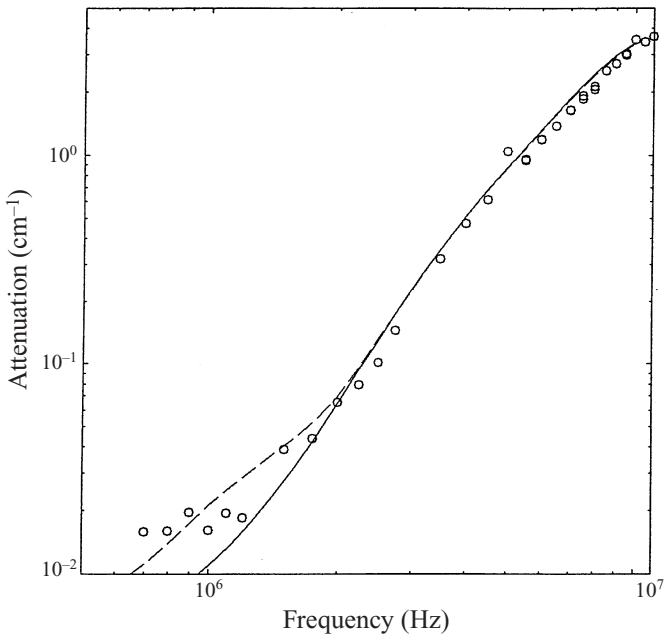

FIGURE 14. Experimental and theoretical results for the attenuation in a mixture of glass particles (mean radius 63 μm and 8.5 μm standard deviation) in glycerol at 0.05 volume fraction. Circles are experiments, solid and broken lines are the theoretical predictions.

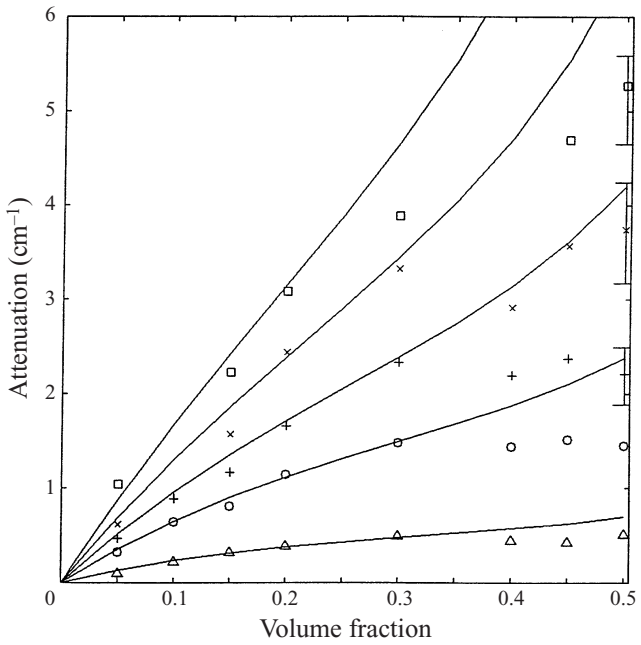

FIGURE 15. Experimental and theoretical results for the attenuation as a function of volume fraction for different frequencies, using the same glass particles and glycerol as in figure 11. Symbols are experiments, solid lines theory for monodisperse particles and broken lines theory for polysdisperse particles. △, 2.5 MHz; ○, 3.5 MHz; +, 4 MHz; ×, 4.5 MHz; □, 5 MHz.

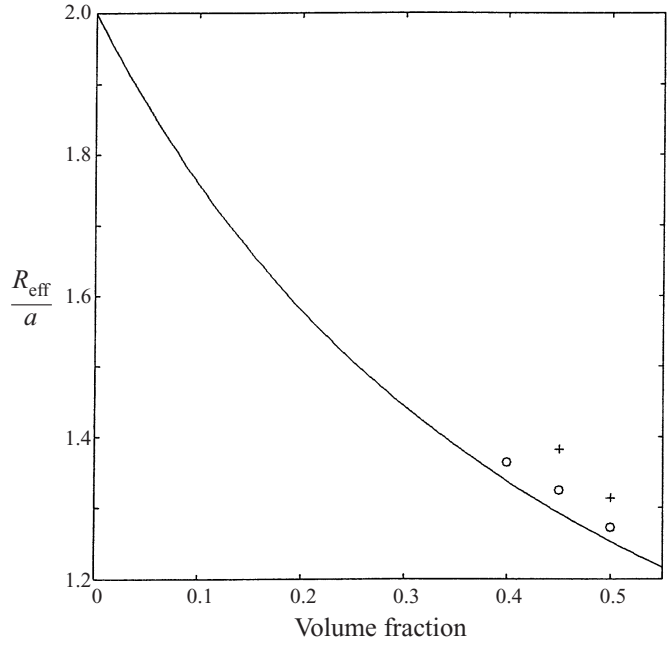

FIGURE 16. Liquid-shell to particle radius ratio as a function of volume fraction. Solid line is (52). Symbols are the values that would have to be used to get very good agreement with the experimental data shown in figure 15 at high volume fractions. ○, 2.5 MHz data; +, 5 MHz.

three times for each f at $\phi = 0.3$ and 0.5. At smaller volume fractions the data were quite reproducible and the error bars were typically smaller than the size of the symbols shown in figure 15. However, larger variations were observed at higher volume fractions as exemplified by the vertical bars around the data points. Although these error bars are quite significant, we see that the theory consistently overpredicts the attenuation for $\phi > 0.3$.

As mentioned earlier, there is some concern about the proper choice of R_i/a_i to be used in the effective-medium approximations for polydisperse suspensions. To see how the choice of R_i/a_i affects the results, we calculated the values of R_i/a_i (assumed to be independent of the particle radius) at which the theory and experiments would coincide for $\phi \geqslant 0.3$ at 2.5 and 5 MHz. The results are shown in figure 16. The solid line in that figure corresponds to the value used in the results presented in figure 15. We see that only slight changes in R/a are needed to make the theory predictions coincide with the experimental data. In other words, the results for the attenuation are very sensitive to the choice of R/a in very dense suspensions. Finally, the fact that the scatter in the attenuation data is significant at higher volume fractions suggests that the attenuation might be quite sensitive to the manner in which the suspension is stirred. As noted earlier we used hand-stirring just before taking the attenuation measurement. Perhaps using a fluidized bed would have produced different attenuation data at high volume fractions.

The comparisons shown so far were dominated by the thermal and scattering effects. Experiments in which the viscous losses are significant were carried out by Hampton (1967), but those were for clay particles which are highly non-spherical. To assess the theory for the viscous regime, we have measured attenuation for a suspension of small glass particles in water. The size distribution for these particles is shown in figure

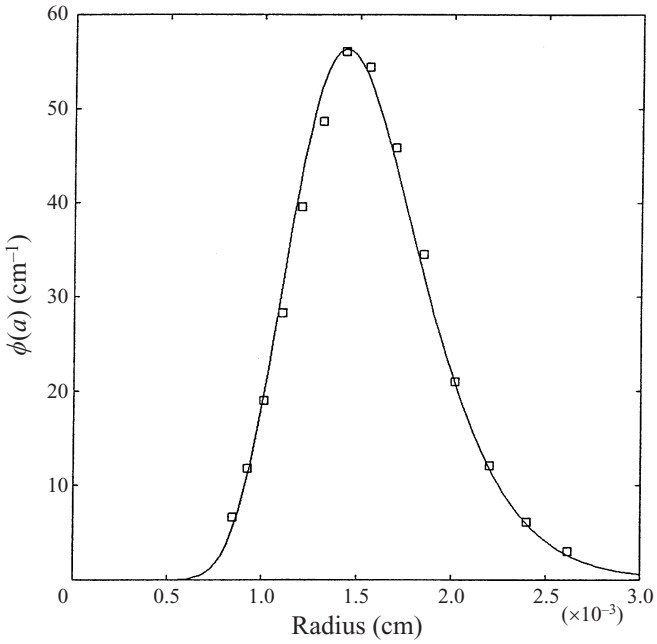

FIGURE 17. Volume-fraction distribution of the glass particles used in figure 18. Circles are measurements, the solid line is a fit using a log-normal size distribution.

17 together with the fit used in the calculations. The mean radius is 15 μm and the standard deviation is 3.5 μm. These particles have a very small terminal velocity and it is not necessary to add glycerol to keep them suspended. For the frequency range over which we could measure attenuation, i.e. for 0.7–10 MHz, the non-dimensional wavenumber $k_{cl}a$ varies from 0.03 to 0.5. The particle-to-liquid (pure water) density ratio in this case is 2.55, and the viscous attenuation dominates the lower part of the frequency range, while the scattering attenuation becomes important at higher frequencies.

The results for volume fractions 0.05, 0.2, 0.3, and 0.4 are shown in figure 18. We see that the measured attenuation is proportional to $f^{1/2}$ in the viscous range, which is to be expected for the case when the Stokes layers are thin compared with the particle radius (see, e.g., Allegra & Hawley 1972). We see an excellent agreement between the theory and experiments. It may be noted that the attenuation does not vary linearly with the volume fraction, indicating that the effective-medium approximation represents a significant improvement over the dilute theory. We also note that, unlike the case of larger particles, the attenuation increases monotonically with the volume fraction for the entire range of frequencies over which the measurements are made.

6. Phase speed

While the physics of acoustics is very interesting, it appears that the determination of the particle volume fraction from acoustic measurements will be, in general, difficult because of the sensitive dependence of the acoustics on physical properties of the particles and liquid and the particle size distribution. Since the phase speed is relatively less sensitive to the particle size, it might be more advantageous to measure the phase speed. The scattering regime can lead to large attenuation and resonance

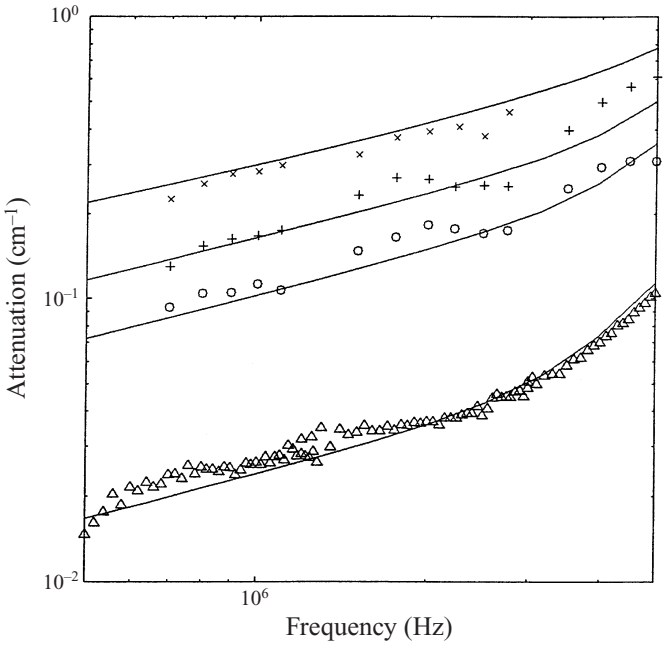

FIGURE 18. Experimental and theoretical results for the attenuation as a function of frequency at different volume fractions, using glass particles in water. Symbols are experiments, solid lines are theory. Volume fractions are △, 0.05; ○, 0.2; +, 0.3 and ×, 0.4.

behaviour sensitive to the mechanical properties of particles. The phase speed near the resonance frequencies can vary significantly. Thus, it is desirable to carry out measurements at low frequencies where the scattering effects will be insignificant.

When $k_{cl}a$ is small the phase speed can be measured for cases for which the Stokes layers are much smaller than the particle radius. In this limit the speed is nearly independent of the particle radius. Figure 19 shows the phase speed as a function of volume fraction in this limit for a glass–water system with two different sizes. Note that the speed is essentially the same for both particle sizes. The attenuation under these conditions would be proportional to a^{-1} (Allegra & Hawley 1972). Figure 19 also shows results for the case when the Stokes layers are much thicker than the particle radius. Once again, in this limit the phase speed is nearly independent of the particle radius while the attenuation would vary significantly with the particle radius as a^2. Note that the phase speed as a function of volume fraction goes through a minimum in the low-frequency limit. The monotonic increase at high frequency might be more suitable for determining the volume fraction. Thus, the ideal frequency for measuring the phase speed corresponds to the one for which the Stokes layers are thin compared with the particle radius and $k_{cl}a$ is small.

7. Summary

We have derived equations for describing small-amplitude acoustic wave propagation through a suspension. The equations are similar to those for a single-phase medium but require closures for estimating the effective properties of the suspension. We used an effective-medium model to solve for the conditionally averaged temperature, density, and velocity fields inside a test particle, and estimated thereby the

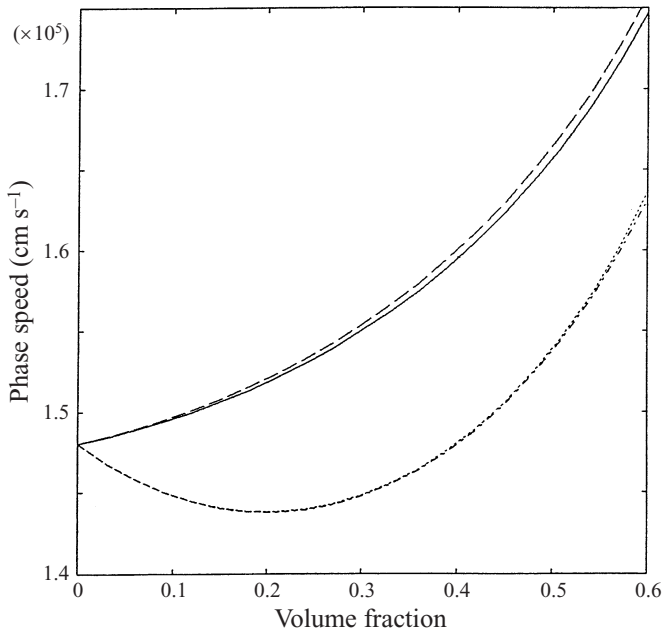

FIGURE 19. Wave speed as a function of volume fraction for two limiting cases. Solid line, $a^2\omega\rho_l/\mu_l = 3 \times 10^3$ and $k_{cl}a = 8 \times 10^{-4}$; long-dashed line the same, but with the particle radius increased by a factor of 5; dashed-dotted line, $a^2\omega\rho_l/\mu_l = 3 \times 10^{-4}$ and $k_{cl}a = 8 \times 10^{-4}$; short-dashed line the same but with the particle radius increased by a factor of 5.

effective properties such as the density, heat capacity, conductivity, viscoelasticity, and compressibility in a self-consistent manner. When the wavelength is large compared with the particle radius the multiparticle interactions in the suspension can be approximated by Stokes or Laplace equations for which a number of effective properties have been determined in recent years through rigorous multiparticle calculations. We show that the estimates obtained using the effective-medium approximation for various properties are in excellent agreement with these rigorous calculations. The theory is also shown to be excellent agreement with the experimental data for the polystyrene–water system by Allegra & Hawley (1972). The ratio of particle radius to wavelength was small in these experiments. To test the theory for larger particles we have conducted experiments both for polystyrene particles and glass particles in water. The agreement with the data for the polystyrene–water system which exhibits several resonances due to shape oscillations is excellent. However, the comparison was limited to dilute suspensions because of the unavailability of concentrated monodisperse suspensions in the particle size range of interest. The glass–water system had significant polydispersity but covered a broad range of volume fractions. The agreement between the theory and experiments for small particles in which the viscous attenuation dominates is excellent while for large particles for which the scattering losses dominate the agreement is good only up to $\phi = 0.3$. At higher volume fractions the attenuation measured in our laboratory decreased, in contrast with the theory prediction.

In view of the remarkable success of the effective-medium approximation in predicting the attenuation in solid–liquid systems, it seems that the procedure used here may also find applications in other acoustic problems, e.g. in the electroacoustics of

colloidal suspensions (O'Brien 1990) and in acoustics of fluid-saturated porous media (Burridge & Keller 1981).

This work was supported by the Department of Energy, Environmental Science Management Program, under Grant DE-FG07-96ER14729. The computations were performed using the resources of NCSA at University of Illinois. AS also acknowledges the support provided by the National Science Foundation under Grant CTS-9632227.

REFERENCES

Allegra, J. R. & Hawley, S. A. 1972 Attenuation of sound in suspensions and emulsions: theory and experiments. *J. Acoust. Soc. Am.* **51**, 1545–1563.

Atkinson, C. M. 1991 Acoustic wave propagation and non-intrusive velocity measurements in highly concentrated suspensions. PhD Thesis, MIT.

Atkinson, C. M. & Kytömaa, H. K. 1992 Acoustic wave speed and attenuation in suspensions. *Intl J. Multiphase Flow* **18**, 577–592.

Bonnecaze, R. T. & Brady, J. F. 1991 The effective conductivity of random suspension of spherical particles. *Proc. R. Soc. Lond.* A **432**, 455–465.

Burridge, R. & Keller, J. B. 1981 Poroelasticity equations derived from microstructure. *J. Acoust. Soc. Am.* **70**, 1140–1146.

Carstensen, E. L. & Foldy, L. L. 1947 Propagation of sound through a liquid containing bubbles. *J. Acoust. Soc. Am.* **19**, 481–501.

Dodd, T. L., Hammer, D. A., Sangani, A. S. & Koch, D. L. 1995 Numerical simulations of the effect of hydrodynamic interactions on diffusivities of integral membrane proteins. *J. Fluid Mech.* **293**, 147–180.

Duraiswami, R., Prabhukumar, S. & Chahine, G. L. 1998 Bubble counting using an inverse acoustic scattering method. *J. Acoust. Soc. Am.* **104**, 2699–2717.

Epstein, P. S. & Carhart, R. R. 1953 The absorption of sound in suspensions and emulsions. I. Water fog in air. *J. Acoust. Soc. Am.* **25**, 553–565.

Gradshteyn, I. S. & Ryzhik, I. M. 1994 *Table of Integrals, Series, and Products*, 5th Edn. Academic.

Hampton, L. D. 1967 Acoustic properties of sediments. *J. Acoust. Soc. Am.* **42**, 882–890.

Jeffrey, D. J. 1973 Conduction through a random suspension of spheres. *Proc. R. Soc. Lond.* A **335**, 355–367.

Ju, J. W. & Chen, T. M. 1994 Effective elastic moduli of two-phase composites containing randomly dispersed spherical inhomogeneities. *Acta Mech.* **103**, 123–144.

Kim, S. & Russel, W. B. 1985 Modelling of porous media by renormalization of the Stokes equations. *J. Fluid Mech.* **154**, 269–286.

Ladd, A. J. C. 1990 Hydrodynamic transport coefficients of random dispersions of hard spheres. *J. Chem. Phys.* **93**, 3484–3494.

Landau, L. D. & Lifshitz, E. M. 1986 *Theory of Elasticity*, 3rd Edn. Pergamon.

Mo, G. & Sangani, A. S. 1994 A method for computing Stokes flow interactions among spherical objects and its application to suspension of drops and porous particles. *Phys. Fluids* **6**, 1637–1652.

Norato, M. A. 1999 Acoustic probe for the characterization of solid-gas-liquid slurries. PhD Thesis, Syracuse University.

O'Brien, R. W. 1990 The electroacoustic equations for a colloidal suspension. *J. Fluid Mech.* **212**, 81–93.

Prosperetti, A. 1984 Bubble phenomena in sound fields: part one. *Ultrasonics* **22**, 69–77.

Sangani, A. S. & Mo, G. 1997 Elastic interactions in particulate composites with perfect as well as imperfect interfaces. *J. Mech. Phys. Solids* **45**, 2001–2031.

Sangani, A. S. & Yao, C. 1988 Bulk thermal conductivity of composites with spherical inclusions. *J. Appl. Phys.* **63**, 1334–1341.

Sangani, A. S., Zhang, D. Z. & Prosperetti, A. 1991 The added mass, Basset, and viscous drag coefficients in nondilute bubbly liquids undergoing small-amplitude oscillatory motion. *Phys. Fluids* A **3**, 2955–2970.

Spelt, P. D. M., Norato, M. A., Sangani, A. S. & Tavlarides, L. L. 1999 Determination of particle size distributions from acoustic wave propagation measurements. *Phys. Fluids* **11**, 1065–1080.

Turner, J. C. R. 1976 Two-phase conductivity, the electrical conductance of liquid-fluidized beds of spheres. *Chem. Engng Sci.* **31**, 487–492.